Intrinsic Diversity In Primary Cilia Revealed Through Spatial Proteomics

Jan N. Hansen [1,2], Huangqingbo Sun [2,*], Konstantin Kahnert [2,*], Eini Westenius [3,4], Alexandra Johannesson [1], Kalliopi Tzavlaki [1], Casper Winsnes [1], Emmie Pohjanen [1], Jenny Fall [1], Frederic Ballllosera Navarro [2], Anna Bäckström [1,2], Cecilia Lindskog [5], Fredric Johansson [1], Kalle von Feilitzen [1], Angelica Delgado Vega [3,4], Mathias Uhlén [1,6], Anna Martinez Casals [2], Diana Mahdessian [1], Anna Lindstrand [3,4], Ulrika Axelsson [1], Emma Lundberg [1,2,7,8,†]

1 Science for Life Laboratory, School of Engineering Sciences in Chemistry, Biotechnology and Health, KTH - Royal Institute of Technology, Stockholm, Sweden.
2 Department of Bioengineering, Stanford University, Stanford, CA, USA.
3 Department of Molecular Medicine and Surgery, Karolinska Institutet, Stockholm, Sweden
4 Department of Clinical Genetics and Genomics, Karolinska University Hospital, Stockholm, Sweden
5 Department of Immunology, Genetics and Pathology, Cancer Precision Medicine Research Unit, Uppsala University, Uppsala, Sweden
6 Department of Neuroscience, Karolinska Institutet, Stockholm, Sweden.
7 Department of Pathology, Stanford University, Stanford, CA, USA.
8 Chan Zuckerberg Biohub, San Francisco, San Francisco, CA, USA.
* Contributed equally

† Correspondence: emmalu@stanford.edu

Abstract

Primary cilia are a critical organelle found on most human cells, and their dysfunction is linked to hereditary ciliopathies with diverse symptoms. Despite their significance, the specific roles of cilia in different cell types remain poorly understood due to limitations in analyzing ciliary protein composition. We employed antibody-based spatial proteomics to expand the Human Protein Atlas to primary cilia. Our analysis identified the subciliary locations of 654 proteins across three cell lines, examining 110,844 individual cilia. We found that 67% of the ciliary proteome is cell-type specific, and 78% exhibited dynamically varied localization patterns, indicating that protein trafficking is crucial for ciliary function. Our findings portray cilia as dynamic sensors tuning their proteome to effectively sense the environment and compute cellular responses. We identified 71 novel cilia proteins and linked a genetic variant in *CREB3* to typical ciliopathy phenotypes. This open, spatial cilia atlas advances research on cilia and ciliopathies.

Introduction

Cilia are small, hair-like cellular appendages that exist on almost any vertebrate cell. They are classified into motile cilia and immotile, primary cilia. While motile cilia move entire cells or fluid flow along epithelial surfaces, primary cilia are immotile and fulfill an antenna function [1]. Most of what we know about the function of primary cilia stems from hereditary diseases that are caused by primary cilia dysfunction, so-called ciliopathies [2]. Ciliopathy patients present with a broad spectrum of phenotypes, including polydactyly, cognitive impairments, obesity, kidney defects, or blindness, underlining that primary cilia fulfill pleiotropic and tissue-specific functions [2]. However, the molecular mechanisms underlying primary cilia function are largely unknown.

Functionally, primary cilia represent an organelle optimized for signal transduction: they sense extracellular cues via receptors, locally transduce the signal, and relay it to the cell body [3]. The primary cilium reportedly participates in several signaling pathways: individual components of Hedgehog signaling, G-protein-coupled receptor (GPCR) signaling, receptor-tyrosine-kinase (RTK) signaling as well as transforming growth factor β (TGF-β) signaling, bone morphogenetic protein (BMP) signaling, and Wnt signaling have been observed to localize to the primary cilium [1]. However, while the molecular sequence of events has been mostly understood only for Hedgehog signaling [1], knowledge about how the other components engage mechanistically in signaling pathways and whether and how the cilium can distinguish between signals of different receptors targeting the same signaling mechanism (e.g., GPCRs) remains elusive [4].

The architecture of the cilium and the process of its construction, called ciliogenesis, has been extensively studied. Two ciliogenesis pathways have been described, the external and the internal pathway, which are initiated by the mother centriole docking to the plasma membrane or a vesicular membrane, respectively [5]. Next, the cilium emerges by extension of the axoneme from the mother centriole. The axoneme is the central skeleton structure of the cilium consisting of nine microtubule doublets nucleated at the centriole. Beyond providing the cilium with a skeleton and thereby determining its length, the axoneme serves as a template for protein trafficking in the cilium, which is driven by the intraflagellar transport (IFT) machinery [1]. Early during ciliogenesis, several protein structures are built around the mother centriole, which let it become the “basal body”, and at the interface of cilium and cell body, which is called the “transition zone” [5]. For example, transition fibers are formed to mount the basal body to the plasma membrane [6–9]. The transition zone serves as a gate limiting exchange of lipids and proteins between cilium and the cell body, which macro-structurally appear as a continuum [10]. The transition zone consists of several protein structures, such as a Septin-based diffusion barrier at the ciliary membrane [11], Y-shaped protein complexes connecting plasma membrane and ciliary axoneme [12], and the distal appendage matrix sealing the space between transition fibers [13]. Yet, the composition and mechanisms of the gate between cilium and cell body remains poorly understood.

Nonetheless, it has been shown that the protein and lipid repertoire of the primary cilium is distinct from the cell body, which is achieved by controlled entry and exit of proteins [14,15]. This tightly controlled shuttling of proteins into and out of the primary cilium fulfills multiple functions: (1) Enabling signal transduction, e.g., during activation of Hedgehog signaling a competitive spatial

exchange of proteins triggers the signaling cascade [16]. (2) Relaying information to the cell body to regulate cellular responses, e.g., in Hedgehog signaling, transcription factors are modified in the primary cilium, shuttle to the nucleus, and instruct a specific gene expression program [16]. (3) Tuning the sensitivity of the ciliary antenna function, e.g., activated GPCRs in the primary cilium are removed from the ciliary membrane and transported out of the cilium [17,18], and the ciliary length determines its sensitivity in mechanosensation [19]. (4) Assembling and disassembling the primary cilium [5]. In conclusion, understanding the ciliary protein repertoire and the underlying spatiotemporal dynamics appears as a key to understanding the antenna function and signaling pathways employed by the cilium, and how the cilium is influenced by and shaping cell states [1].

A major limitation for primary cilia research is imposed by the size of the primary cilium. Its volume can be approximated to be in the range of 0.3 fl, which is more than 1,000-times smaller than the cell body, thus requiring highly sensitive measurement technologies. In addition, extracting and purifying intact cilia is difficult, if not impossible, because the ciliary membrane is a continuum of the plasma membrane [5]. Thus, the ciliary proteome has mainly been characterized using proximity-labeling-based spatial proteomics techniques, such as APEX-, BioID, or Turbo-ID-based proximity labeling [20–24]. However, the use of proximity-labeling MS features several disadvantages: (1) it does not provide single cell resolution and results represent a mix of cilia in multiple signaling states; (2) technologically, it can only reveal ciliary protein enrichment compared to the cell body; (3) it is not functional in all cell types due to endogenous enzymatic activity; (4) it relies on fusing an enzyme, such as APEX or TurboID, to a ciliary GPCR or ciliary protein fragment, which may bias signaling in the primary cilium; and (5) it is not applicable to study human tissues.

Here, we overcome this challenge and shed light on the physiological function of individual primary cilia on human cells by applying large-scale antibody- and imaging-based spatial proteomics. We establish a new resource for the cilia field: a section in the public Human Protein Atlas (HPA) that provides high-resolution confocal 3D images and subciliary annotations for 654 cilium-localizing proteins in three ciliated cells of diverse origin. We reveal that the primary cilium shows the most heterogeneous proteome compared to all other organelles, across cell types and within the same cell population, and that the diversity relates to cell-individual customization of the cilium to conduct cell-specific sensory signaling. Furthermore, we demonstrate that our cilia atlas paves new avenues for cilia and ciliopathy research, by leveraging its content for revealing a new cilia marker and identifying a potential novel ciliopathy gene.

Results

Mapping the subcellular and subciliary location for human proteins

To examine the proteomic composition of primary cilia on the single-cilium level, we developed an antibody-based spatial proteomics workflow, which applies the antibody library of the Human Protein Atlas (HPA) [25,26] in a co-staining approach with markers for nuclei, cilia, and basal bodies (Fig. 1A) and high-throughput, high-resolution 3D confocal microscopy (Fig. 1B). With this workflow we comparatively analyzed three immortalized primary human cell lines of different tissue origin and sex: (1) starved hTERT-RPE1 cells from the embryonic retina [27], to represent the best studied *in vitro* model for human cilia, (2) RPTEC/TERT1 cells [28], derived from the epithelial kidney proximal tubules, to represent a cell type affected in the most common ciliopathy - polycystic kidney disease (PKD), and (3) the mesenchymal, multipotent, stromal ASC52telo cells [29], derived from adipose tissue, to represent a multipotent cell type. The three cell lines are morphologically diverse and likely rely on different signaling and ciliogenesis programs, allowing coverage of a broad band of cellular functionality and ciliary diversity (Fig 1C). The starved hTERT-RPE1 cells represent a synchronized culture with a high ciliation rate and that generates cilia mostly at the cell-glass-interface (Fig 1D). Reportedly, hTERT-RPE1 cells predominantly employ the internal ciliogenesis pathway [5]. The RPTEC/TERT1 cell culture generates polarized cells that cycle slowly and grow long cilia sticking into the fluid (Fig. 1D). In contrast, the ASC52telo cells cycle fast and present short, flat-lying cilia (Fig. 1D). We observed ASC52telo cells to occasionally show dots or small lines of the ciliary marker on one centrosome during mitosis, hinting to the retainment of a ciliary vesicle or cilium during mitosis, similar to reported observations in HEK293T cells [30] (FIG 1E). This was not observed in the other cell lines. However, in RPTEC/TERT1 cells, we occasionally observed cells that formed two adjacent cilia (Fig. 1F). Double ciliation was also seen in hTERT-RPE1 cells, albeit much rarer (Fig. 1G). Interestingly, we also once observed a ciliary bridge in RPTEC/TERT1 cells, where cilia from neighboring cells appeared to be either connected or touching (Fig. 1H).

For the targeted antibody-based spatial proteomics approach, we assembled a list of candidate proteins based on existing curated databases including SYSCILIA gold standard version 2 [31] and the ChlamyFP.org database [15], the tissue resource of the HPA [25,32], MS data sets on primary cilia based on proximity-labeling approaches or purification attempts [20–24,33], predictive studies including the CiliaCarta [34–36], comparative transcriptomics studies [37], phylogenetic studies on flagellated species [38,39], CRISPR screens [40,41], MS studies of flagella or motile cilia [42–46], Cryo-ET studies of sperm flagella [47–49], and studies of the centrosomal proteome [50–55]. For a strong focus on signaling pathways, we extended the screen with key components of diverse signaling pathways, such as AKT kinases, MAP kinases, mTOR, a selection of G-protein coupled receptors (GPCRs), phosphodiesterases (PDEs), or adenylyl cyclases, even without any prior evidence of localizing to cilia. Interestingly, our assembled cilia candidate list highlighted that nearly ten thousand protein-coding genes have been reported or suggested to potentially produce proteins localizing to primary cilia or engaging in their regulation (Fig. 1I, Supplementary Table 1). The overlap of proteins identified in cilia with different methods or in different cell types or species was particularly small: 4122, 1905, and 1011 genes were attributed to cilia in one, two, or three data

sets only, respectively (Fig. 1I). This points to an incredible heterogeneity in the ciliary proteome across species and cell types and potentially many false positives due to technical limitations. Finally, we prioritized the candidate list and selected 1,935 candidate proteins for assessment of ciliary localization in human cells (see Materials and Methods) (Fig. 1J, Supplementary Table 2).

A spatial map of the human cilia proteome

Applying our spatial proteomics data generation pipeline for revealing 1,935 proteins in ciliated cells produced a massive high-resolution 3D confocal image data set of cilia and their protein composition with 17,115 3D image stacks, revealing 236,504 cells, 110,844 of which displayed a cilium. We applied the established HPA subcellular workflow to annotate all images, which involves investigation and review of every staining by multiple skilled cell biologists.[26] In addition to the 35 subcellular organelles and structures annotated in the HPA, we annotated protein localization to the primary cilium, basal body, transition zone, and ciliary tip (Fig. 2A,B). We could identify the proteins encoded by 654 of our 1,935 candidate genes at cilia, of which 352 proteins were detected in primary cilia, 59 at the ciliary tip, 95 at the transition zone region, and 403 at the basal bodies (Fig. 2C). Furthermore, we observed additional subpatterns of ciliary localization, such as partial staining of the proximal cilium (e.g., for EFCAB7, EVI2A, and TRIM46, Fig. 2D), which might correspond to a domain distal from the transition zone and close to the “inversin” compartment [56], such as the EVC-EVC2 complex described in mouse fibroblasts [57], or a staining of the ciliary pocket; spotty staining patterns along the cilium (e.g., for TRIO, Fig. 2D); or enrichment towards the ciliary tip (e.g., for C2CD4C, Fig. 2D); or combinations of spotty patterns and enrichment towards the tip for the same protein (e.g., for TMEM237, Fig. 2D), highlighting the subciliary resolution of our screen.

Among the revealed proteins are many established ciliary proteins, such as the intraflagellar transport protein IFT22, SMAD7 localizing to the basal body, the subdistal appendage protein CEP164, the MKS-complex protein TCTN2 at the transition zone, the small GTPase RAB7A in the transition zone, the ciliary trafficking protein ARL6 enriched towards the ciliary tip, the kinesin KIF7 at the ciliary tip, the septin SEPTIN2, the adenylyl cyclase ADCY3, or the small GTPases RAB23, which is known to participate in regulating GLI transcription factors and ciliary Hedgehog signaling (Fig. 2E). [58,59] This confirms the validity of our approach for diverse types of ciliary proteins and provides the cilia field with subcellular resolution pictures of these and many more known proteins in unperturbed human cells. In total, we identified as much as 71 proteins that had never been previously associated with any type of cilium across different species (Fig. 2F, Supplementary Table 3). Additionally, there were 193 proteins that had never been identified to localize to human cilia by MS- or Cryo-ET based approaches (Fig. 2G), and 96 proteins that had never been validated to localize to cilia (Fig. 2H). Notably, for those proteins that were identified only by MS-based approaches, the subciliary localization was not known, whereas we provide subciliary localization resolution.

An interesting new discovery were three proteasomal subunits in cilia: PSMD10, PSME3, and PSMA6 (Fig. 2I). PSMD10 is among the 71 proteins never related to cilia before. PSME3 has previously been detected in one mouse sperm flagella data set [47] and was bioinformatically predicted to be a cilia protein [34]. PSMA6 was identified in cilia by many approaches and was listed

in databases [15], an analysis of murine kidney cilia with cilia-APEX [22], a CRISPR-based screen [41], a comparative transcriptomic analysis [37], and in motile cilia and sperm flagella studies [42,45,47–49]. Other examples for our data confirming proximity-labeling-MS-approaches in the cilia of model organisms are ZNF330 or the senescence-regulator RSL1D1 (Fig. 2J), which both had previously been identified by cilia-APEX in murine kidney cells [21,22]. Also, we confirm previous bioinformatic predictions, such as ARL15 in cilia (Fig. 2J) [36]. Some of the studies in our candidate list analysis were from motile cilia. Surprisingly, we identified proteins believed to be specific for motile cilia in primary cilia of RPTEC/TERT1 cells, such as the central-pair protein HYDIN, IQCA1, which is part of the nexin-dynein-regulatory complex in motile cilia, or the CATSPER2 channel subunit (Fig. 2K). This is particularly interesting in light of recent descriptions of motile cilia proteins and active motility of primary cilia in *ex vivo* pancreatic islet cells [60]. Yet, we see that HYDIN, IQCA1, and CATSPER2 accumulate towards the tip rather than show staining along the whole cilium, which might indicate for HYDIN and IQCA1 that they are not in fact implemented into the axoneme but might just transit the cilium. Of note CATSPER2 is expressed in RPTEC/TERT1 cells according to the HPA cell line sequencing data confirming staining validity. Further studies will need to delineate why and to which purpose motile cilia proteins transit RPTEC/TERT1 cilia and whether this finding translates to primary cilia of proximal tubule cells *in vivo*. However, kidney proximal tubule cells of patients with kidney injury have been observed to feature multi-ciliated cells whose cilia ultra-structurally show features of motile cilia [61], indicating that proximal tubule cells may in fact be able to establish ciliary motility.

The primary cilium is a hub for diverse sensory signaling pathways

To explore the functions of the human cilia proteins, we performed an enrichment analysis for Gene Ontology (GO) Biological Process terms (Supplementary Fig. 1, Supplementary Table 4). Beyond many terms relating to maintenance processes of the cilium or basal body (e.g. intraciliary transport, adj. p=1.1906e-27 and cilium organization, adj. p=4.7218e-94), we found significant enrichment of terms relating to signaling, such as calcium signaling (calcium-mediated signaling, adj. p=0.0008), Wnt signaling (Wnt signaling pathway, adj. p=0.0006), cAMP signaling (cAMP-mediated signaling, adj. p=0.0028), and morphogenesis and developmental signaling pathways (e.g. regulation of developmental growth adj. p=0.0054) (Fig. 3A, Supplementary Table 4). In fact, we detected signaling proteins of most major signaling pathways in the primary cilium (Table 1) of which many had hitherto not been confirmed in cilia. For example, we revealed in cilia the kinases AKT1 and AKT3, the Serine/threonine-protein kinase TAO1 (TAOK1), a catalytic and regulatory subunit of PI3K (PIK3CA and PIK3R4), the focal adhesion kinase PTK2, the calcium/calmodulin dependent protein kinase CAMK1G, the protein phosphatase 2 (PPP2R3C), the E3 ubiquitin-protein ligase MIB1, the vascular endothelial growth factor receptor 3 FLT4, the GPCR OPRL1, the src-related receptor PDGFRA, the transforming growth factor beta receptor 1 TGFBR1, and the cyclic nucleotide gated ion channel CNGA2 (Fig. 3B). Another example is the Triple functional domain protein TRIO mentioned above (Fig. 2D), a Guanine nucleotide exchange factor (GEF) for RHOA and RAC1 GTPases [62] and which reportedly mediates signal transduction in the recently discovered axon-cilium-synapse [63]. In conclusion, these results demonstrate that the cilium is a versatile signaling organelle with broad signaling capacities, filled with most receptor types and diverse downstream signaling machinery. The fact that we do not only find receptors but also downstream central signaling hubs like AKT1 emphasizes that the cilium is not

just a sensor but also a computer, processing signals into a response that it ultimately relays to the cell body.

Table 1 Signaling proteins revealed in cilia or basal bodies

Gene names part of the selected GO terms are shown if they were revealed at the Primary Cilium Tip, Primary Cilium, Primary Cilium transition zone (TZ), or the Basal Body.

Signaling pathway (Gene ontology = GO term)	**Primary Cilium Tip**	**Primary Cilium**	**Primary Cilium TZ**	**Basal Body**
G-protein coupled receptor signaling pathway (GO:0007186)	CAMK2A, ADCY2, OPRL1	ATP2B4, CAMK2A, PRKACA, ACTN2, TULP3, ADCY2, PDE4D, GPR83, OPRL1, ADCY3, LGR5, AKT1, PRKACB, GPR161, HTR7, GPR180, ADCY9, ADORA1, FZD6, ADRB2, PTAFR, ROBO1, GPRC5C, INSR, LPAR3, MRGPRF, ADCY5, FZD4, SPHK1, FZD8, CHRM2, PDE4B, SSTR3	CAMK2A, ACTN2, TULP3, ADCY3, LGR5, GPR161, GPRC5C, INSR, MRGPRF, SPHK1	ATP2B4, GNAI3, PRKACA, TULP3, RAPGEF4, RPGRIP1L, NHERF1, GNAI2, TACR1, PRKD3, GPR83, GNAI1, PLCB2, ADCY3, LGR5, AKT1, PRKACB, ADCY9, ADGRV1, FZD6, TUB, ADRB2, TAPT1, INSR, FZD2, CHRM2, FFAR4, ADRB3, GABBR1, LGR4, GNAT3
cAMP-mediated signaling (GO:0019933)	ADCY2, OPRL1	ADCY2, PDE4D, OPRL1, PDE11A, PDE4B		PDE4C, CREB1, GNAI1, PDE11A, PDE6B, PDE5A, FFAR4, PDE4C
Calcium-mediated signaling (GO:0019722)	OPRL1, PDPK1, CAMK2D, GSTM2	ATP2B4, PRKACA, FKBP1B, OPRL1, PRKAA1, PDGFRA, PDPK1, CAMK2D, CACNA1C, RCAN2, ATP2A2, SPHK1, PPP3R2, GSTM2, PPP3R1, ACTN3	CAMK2D, SPHK1, GSTM2, ACTN3	ATP2B4, PRKACA, FKBP1B, PLCG1, PRKAA1, CAMTA1, LRRK2
Receptor tyrosine kinase signaling pathway (GO:0007169)	WDR54, NR1H4, CHRNA3, MAPK1, MAPK3, PDPK1, PTK2, PIK3CD	WDR54, NR1H4, FLT4, RAB7A, FGFR1, CHRNA3, MAPK1, MAPK3, IFT20, WNT5A, PIK3CA, DNAI1, BMP2, PRKAA1, PDGFRA, AHI1, MAP2K5, IGF1R, PDPK1, AKT1, EGFR, BRAF, CTNNB1, ADRB2, PTK2, ROBO1, INSR, PIK3CD, FZD4, GRB2	RAB7A, CHRNA3, BMP2, INSR	PRKCZ, FGFR1, CHRNA3, MAPK1, MAPK3, TGFB1, NHERF1, IFT20, GNAI2, CCDC88A, TEK, PLCG1, PRKAA1, MAP2K5, PRICKLE1, AKT1, RASA1, EGFR, BRAF, MAPKAPK2, CRK, CTNNB1, MAP2K1, ADRB2, INSR, HRAS
Transforming growth factor beta receptor signaling pathway (GO:0007179)	TGFBR1, PDPK1, SMAD4, PTK2	FKBP1A, AXIN1, TGFBR1, STK11, BMP2, SMAD6, PDPK1, SMAD4, SMAD3, PTK2, SMAD2, PPARA	BMP2, SMAD3, SMAD2	FKBP1A, SMAD7, TGFB1, SMAD6, SMAD4, SMAD3, PPARA
Vascular endothelial growth factor receptor signaling pathway (GO:0048010)	PTK2	FLT4, PTK2, ROBO1, FZD4		MAPKAPK2

MAPK cascade (GO:0000165)	WDR54, MAPK1, PSMD10, MAPK3, SMAD4	WDR54, MAP4K5, FLT4, MAPK6, FGFR1, CYLD, IGBP1, MAPK1, MAP1LC3A, PSMD10, MAPK3, AXIN1, WNT5A, BMP2, PDGFRA, MAP2K5, IGF1R, SMAD4, EGFR, BRAF, TAOK1, ADORA1, SMAD3, CDC42EP5, CTNNB1, ULK4, ADRB2, ROBO1, PKHD1, INSR, LPAR3, SPHK1, GRB2, AIDA, PJA2	CYLD, BMP2, SMAD3, ULK4, INSR, SPHK1, PJA2	PRKCZ, DLG1, FGFR1, TP73, CYLD, IGBP1, MAPK1, MAPK3, TGFB1, NHERF1, GNAI2, TEK, MAP2K5, PELI2, SMAD4, EGFR, BRAF, DVL3, ATF3, MAPKAPK2, SMAD3, CRK, CTNNB1, MAP2K1, ADRB2, PKHD1, INSR, HRAS, AIDA, FFAR4, ADRB3, LRRK2, PJA2
TOR signaling pathway (GO:0031929)	MAPK3, VHL	PRKACA, MAPK3, AKT3, STK11, MAPKAP1, PIK3CA, PRKAA1, VHL, AKT1, PRKACB, TSC1, PKHD1	TSC1	PRKACA, MAPK3, USP4, CCDC88A, AKT3, PRKAA1, AKT1, PRKACB, PRKAA2, TSC1, PKHD1
BMP signaling pathway (GO:0030509)	MAPK3, SMAD4	MAPK3, WNT5A, BMP2, SMAD6, SMAD4, SMAD2	BMP2, SMAD2	SMAD7, MAPK3, SMAD6, SMAD4
Wnt signaling pathway (GO:0016055)	TTC21B, SMAD4, VCP	CYLD, AXIN1, IFT20, ARL6, NPHP3, WNT5A, STK11, INVS, TTC21B, BMP2, PRKAA1, LGR5, CSNK1D, SMAD4, EGFR, TMEM237, GRHL3, FZD6, VCP, SMAD3, DAPK3, CTNNB1, FZD4, FZD8	CYLD, BMP2, LGR5, TMEM237, VCP, SMAD3	MKS1, CYLD, TGFB1, NHERF1, IFT20, GLI1, INVS, TTC21B, MACF1, PRKAA1, PRICKLE1, LGR5, SMAD4, EGFR, DVL3, PRKAA2, FZD6, VCP, SMAD3, CTNNB1, RUVBL1, FZD2, RUVBL2, LRRK2, CTNND1, LGR4
Notch signaling pathway (GO:0007219)	NR1H4	NR1H4, MIB1, CDKN1B, BMP2, AKT1, PRKCI, ROBO1	CDKN1B, BMP2	IFT74, MIB1, CDKN1B, AKT1
Rho protein signal transduction (GO:0007266)		RHOU, CDC42EP5, ROBO1, ARHGAP1, SEMA4D	SEMA4D	TEK, SHTN1, SEMA4D, LRRK2

Subcellular protein multilocalization and the implications for ciliary function

Protein localization is in general closely associated with protein function. We and others have previously shown that more than half of the human proteome are localized to multiple subcellular compartments, i.e. are multilocalizing [26,64,65]. Here we show that cilium-localizing proteins (including tip and transition zone) are significantly more multilocalizing than other proteins (p=3.7932e-202) - as much as 99% of cilium-localizing proteins are also found in other cellular compartments (Supplementary Fig. 2). Looking at individual stainings, we observed in 90% of the stainings that the protein was multilocalizing to a ciliary and another subcellular compartment in the same cell culture, the most common other compartments being basal bodies, cytosol, nucleoplasm, and microtubules (Fig. 3C). In light of the basal body being the access point to the cilium [10], it makes sense that we observed many proteins also at the basal bodies, since these are transiting the basal body during transport to cilia. Multilocalization with microtubules may indicate that those proteins are part of the ciliary axoneme, a microtubule-based structure.

In contrast, proteins localizing at cilia and in the cytosol and nucleoplasm may rather be proteins involved in relaying information from the cilium to the cell body or potentially engaging in similar or different functions or signaling pathways in different places in the cell (a process called "moonlighting" [66]. In fact we identified kinases that are central in many signaling pathways in cilia, but also in cell body compartments, i.e., the cytosol, such as AKT1 and AKT3, PIK3CA and PIK3R4, or PTK2 (Fig. 3B). Their ability to localize to multiple locations may be attributed to their capacity to transduce distinct signals in various cellular compartments, influenced by the diverse environments with varying stimulators and substrates. We also observed proteins with different ciliary and cell body functions in multiple locations in the cell. For example, the protein TULP3 is well known for a role as a cargo-adaptor in IFT-A mediated trafficking of GPCRs and ARL13B to the cilium [67–69], but may also act as a transcription factor residing at the plasma membrane and relocalizing to the nucleus upon activation [70]. In agreement, we detected TULP3 in cilia, at the plasma membrane, and in the nucleus (Fig. 3B). Many multilocalization observations of cilia proteins may also relate to the cilium relaying information to the cell body. For example, for Gli transcription factors in Hedgehog signaling it is established that post-translational modification of the transcription factors occurs in the cilium, upon which they are transported into the cytosol, where they are - depending on the modification - either degraded or sent to the nucleus to adjust gene transcription [1]. We in fact found additional transcription factors at cilia, such as CRX in cilia (Fig. 3D), or ATF3 and CREB1 at the basal body (Fig. 3D), which co-localized to the nucleoplasm, supporting the hypothesis that the cilium controls gene expression by local modification of transcription factors beyond Sonic Hedgehog signaling, as shown recently for CREB1 [71].

Another class of proteins that often multilocalize and "moonlight" are enzymes, as we recently demonstrated [72]. Little is known about metabolic and enzymatic activities in the cilium. Notably, not only the proteomic but also the lipid composition of the cilium uniquely makes up the ciliary compartment [73]. While the lipid composition of cilia has been shown to be unique compared to the plasma membrane, the processes involved in its formation - whether through transport mechanisms or local production - remain underexplored. While for phosphoinositides it has been demonstrated that the membrane composition is locally regulated by enzymes, for other lipid species it is not understood how they end up in the ciliary membrane, such as for cholesterol, which is described to essentially regulate Hedgehog signaling [73,74]. Interestingly, we discovered several enzymes in cilia, which also localize to other positions in the cell. For example, an enzyme that is part of sterol synthesis, HSD3B1/HSD3B2 (Fig. 3E). Other examples are the Glutathione S-transferase LANCL1, the Inositol polyphosphate 5-phosphatase OCRL, the carboxypeptidase AGBL5 involved in tubulin de-glutamylation and has been indicated as a negative regulator of ciliogenesis [75], the Sphingosine kinase SPHK1, which regulates ceramide levels and is highly engaged in signaling [76–78], or the UDP-glucose glycoprotein glucosyltransferase 1 (UGGT1), a protein that reportedly acts as a gate-keeper for folding of glycosylated proteins at the endoplasmic reticulum (ER) (Fig. 3E) [79,80].

Our data demonstrates that cilia mainly contain multilocalizing proteins and in fact possess a local metabolic machinery, supporting the hypothesis that the ciliary lipid composition is shaped and adjusted locally through enzymatic activity.

Cilia proteomes reveal cell type specific functional differences

Most of the investigated proteins (67%) specifically localized to cilia only in one or two of the studied cell lines (Fig. 4A). In the cell lines where we did not observe ciliary localization, the protein was not detectable or localized to other compartments. For example, we identified the calmodulin- and kinase-related signaling protein STRN3 at the plasma membrane / actin cytoskeleton in all three cell lines, but only in RPTEC/TERT1 cells in the cilium and we identified the common kinase PI3K (PIK3CA) in cilia in RPTEC/TERT1 and hTERT-RPE1 cells but not in ASC52telo cells (Fig 4B). Other examples are the activin receptor ACVR1B, the SEPTIN9, the RHO GTPase activating protein ARHGAP1, or the adenylyl cyclase ADCY3. We observed ADCY3 to be more enriched in cilia of ASC52telo cells than of RPTEC/TERT1 cells, while it co-localized to the plasma membrane in both cell lines. In hTERT-RPE-1 cells, ADCY3 was confined to basal bodies, similar to a previous report [81] (Fig. 4B). Such cell-type specificity of ciliary protein localization is higher than for other organelles and highlights that the ciliary proteome is much more regulated than other organelles and compartments.

In a comparative GO term enrichment analysis of the identified cilia proteins between cell lines (Fig. 4C, Supplementary Fig. 3-4, Supplementary Table 5) we confirmed that indeed each cell line has some unique ciliary specializations. While all cell lines shared GO terms relating to general cilia processes such as (1) ciliogenesis, microtubules, and anchoring of the cilium, (2) transport processes, (3) smoothened signaling, (4) development, and (5) cell polarity (Fig. 4C, Supplementary Fig. 4), we also identified cell type specific processes: RPTEC/TERT1 cilia appeared to be tailored to various sensory signaling pathways, while hTERT-RPE1 cilia appeared to be focused on developmental functions, and ASC52telo cilia appeared to be involved in metabolic activity. Looking into individual GO terms revealed also the specific enrichment for the term “establishment of spindle orientation” (adj. p=0.0050) in ASC52telo cilia, supporting our observation that ASC52telo - in contrast to RPTEC/TERT1 - often retain a primary cilium or ciliary vesicle in mitotic cells (Fig. 1E) and indicating an engagement of cilia in asymmetric cell division processes of pluripotent cells.

Since this study is limited to three cell lines, we expect this heterogeneity to be even higher when extending to more cell types. Notably, the cell type specific ciliary functions align well with the cellular functions of the individual cell lines. RPTEC/TERT1 cells are kidney epithelial cells with their cilia floating in the urine where they may sense hormonal and urine-compositional changes via GPCRs and RTKs to instruct the cell to furnish the cell surface with adequate transporters establishing fine-tuned water and ion homeostasis. hTERT-RPE1 cells show enrichment for processes related to developmental pathways, which might be a consequence of the serum starvation driving them into cell fate changes or senescence. ASC52telo cells have multi-potent features and may require cilium-assisted asymmetrical cell divisions to retain cells with stemness. Of note, we detected ciliary-motility related proteins, like Hydin, IQCA1, or CATSPER2 only in RPTEC/TERT1 cells and their cilia (Fig. 2K) but not in hTERT-RPE1 or ASC52telo cells, highlighting that - if some primary cilia have ciliary motility - it may be a tool employed not by all but only some cell types.

Extensive spatiotemporal dynamics of ciliary proteins

Thanks to the single cell resolution of our imaging-based approach, we were able to assess variations in protein localization and abundance within primary cilia at the individual cell level. Beyond heterogeneity across cilia in different cell types, we also observed an incredible heterogeneity on the single cell level. 345 of 443 (78%) of the primary cilium, primary cilium tip, or primary cilium transition zone stainings were classified as varying across individual cells. While our images reflect a static snapshot, this heterogeneity indicates dynamic spatiotemporal variations of the ciliary state. Using a comparative GO term enrichment analysis, we explored which processes are particularly stable and which are particularly diverse across individual cilia. As expected, proteins engaging in ciliogenesis, microtubules, and ciliary transport-associated processes appeared in both groups, stable and dynamic (Fig. 4D, Supplementary Fig. 5-6, Supplementary Table 6), while the most dynamic localization was observed for proteins involved in signaling, developmental, and morphogenesis processes. As an example for ciliogenesis-related single-cell heterogeneity, RAB8A and RAB34, which are both known to shape the cilium during ciliogenesis by mediating transport of proteins to the growing cilium, localized only to individual cilia (Fig. 4E). Interestingly, some GPCRs showed varying abundance levels across cilia even in the serum-starved, synchronized hTERT-RPE1 cells - e.g., LPAR3, SSTR3, and HTR7 largely varied in ciliary abundance whereas ADRB2 appeared more stable (Fig. 4F). Furthermore, many enzymes in cilia showed spatiotemporal variation, such as for HSD3B1/HSD3B2, SPHK1, and AGBL5 (Fig. 4F). Besides locally contributing to shaping a specific lipid environment, such enzymes may also engage in the process of lipid-dependent regulation of signaling, such as for Hedgehog signaling, which has been shown to be regulated by cholesterol [74,82]. Single-cell variation was also seen for Septins, such as for SEPTIN3, which we newly identified in cilia and which heterogeneously localized to hTERT-RPE1 cilia but not to cilia of the other cell lines (Fig. 4F). Septins are known to be cell type specific and attach to the membrane in a PIP-dependent manner [83]. Observing Septin heterogeneity in single cilia may highlight even more the spatiotemporal dynamics of ciliary lipid-protein-interactions. In conclusion, variation in ciliary localization of GPCRs and lipid-metabolic or -interacting enzymes may relate to the signaling activity of cilia or to fine-tuning of the ciliary signaling machinery.

For some proteins, we observed the variation to correlate with localization of the protein to other cell compartments, or cell cycle stage, such as for CKAP2, where localization to the cilium and part of the microtubule cytoskeleton were seen in some cells, and localization to vesicles in other cells (Fig. 4G). This localization heterogeneity likely relates to the cell cycle, since postmitotic cells showed high intensity for the vesicle staining. A transitional stage where the cilium showed staining for CKAP2 only at the shaft could also be seen. Further confirming that this heterogeneity may relate to the cell cycle, a similar staining variety among ASC52telo cells was observed, whereas, in hTERT-RPE1 cells, which were starved and thus, synchronized, the variation was not visible, instead only the stage with microtubules and cilia staining was observed (Fig. 4G).

In summary, compared to other organelles and cellular structures, the primary cilium displays remarkable heterogeneity in multiple regards, both in terms of cell type specificity and in terms of cell-to-cell heterogeneity and subciliary distribution. Altogether this supports the importance of the cilium in being the cellular antenna and computing unit for sensing the environment and

computing cellular responses, and suggests that that the cilium is tightly controlled by extensive spatiotemporal regulation of the ciliary proteome.

Ciliary subcompartments with unique cellular functions

Spatiotemporal regulation is not limited to cilium versus other cellular compartments, but occurs also within the cilium. The existence of subciliary microdomains for further signaling organization has been suggested [1]. In our manual annotation scheme we distinguished four different types of ciliary domains: tip, cilium, transition zone, and basal body, for which a comparative GO Biological Process enrichment analysis contrasted against cell body regions revealed GO terms uniquely attributable to each subciliary regions (Supplementary Fig. 7A-B, Supplementary Fig. 8). Yet, thanks to the high spatial image resolution in our data set, we could explore subciliary protein localization beyond this manual scheme through CiliaQ-based image analysis [84]. We used CiliaQ to create protein localization profiles for each cilium. The profiles confirmed our annotation scheme and showed a high variance for each annotation class, especially when including multilocalizing proteins (Supplementary Fig. 9A-B). This variance is a consequence of the diverse subciliary localization patterns that we observed (Fig. 2D), and of the heterogeneity on the single cell level as well as the multilocalization of proteins, both demonstrated above for signaling proteins (Fig. 3B) and enzymes (Fig. 3E).

To unbiasedly explore subciliary protein localization patterns and scrutinize the existence of subciliary microdomains, we computed average ciliary localization profiles for each protein and cell line and hierarchically clustered these profiles (see Materials and Methods, Supplementary Fig. 9B, Supplementary Table 9). In fact, localization patterns could be distinguished into at least 20 different kinds per cell line. The localization clustering aligned with distinct molecular and cellular functions of the proteins: For example, a cluster of ciliary intensity profiles in ASC52telo cells related to adenylyl cyclases (GO:0004016, “adenylate cyclase activity”, p=0.04). Furthermore, clusters of ciliary intensity profiles in RPTEC/TERT1 cells related to renal system development (GO:0072001, p=5.2e-05), or tube morphogenesis (GO:0035239, p=0.0002) and Wnt signaling (GO:0060070, “canonical Wnt signaling pathway”, p=0.02) (Supplementary Fig. 9B, Supplementary Table 9). Profiles with high intensity at the cilium just above the transition zone were related to protein localization to the ciliary membrane (GO:1903441, “protein localization to the ciliary membrane”, p=0.03) in RPTEC/TERT1 cells. And profiles enriched below the ciliary tip were enriched for proteins engaging in “protein autophosphorylation” (GO:0048793, p=0.01) like TAOK1 (Fig. 3B). Our analysis demonstrates that proteins involved in similar molecular and cellular functions show characteristic ciliary localization patterns, supporting the existence of ciliary microdomains. Based on the stunning heterogeneity in the presence of proteins in cilia that we observed, we propose that such ciliary microdomains may be transient and their composition may be dynamic.

A stable protein marker for cilia

Given the multilocalizing and heterogeneity aspects of ciliary proteins it is particularly difficult to find suitable marker proteins for cilia imaging assays. A cilia marker protein that is stably and exclusively localizing to primary cilia could greatly aid in identifying cilia in tissues and cells in

research. The common cilia markers such as ARL13B, ADCY3, and acetylated tubulin all come with the disadvantage of being signaling molecules and/or also localizing to other subcellular structures, which makes it hard to apply them in some cell types, where the non-ciliary aspect of these proteins is dominating. ADCY3 antibodies appear to not label consistently cilia on all cell types [81,85], in line with our own observation of a high diversity of ADCY3 localization across the three studied cell lines (Fig. 4B). ARL13B also has cytosolic roles [86,87], and, in particular, posttranslational tubulin modifications of the axonemal cytoskeleton, i.e., acetylation, are known to be heterogeneous across cell types and also strongly label cytoskeletal structures in some cells, i.e., neurons [85,88]. In this study, only one single protein - besides the established marker ARL13B - was stably and exclusively localizing to cilia, across all three cell lines: CFAP300 (Fig. 5A). Mutations in *CFAP300* have been recently reported in patients with motile ciliopathy phenotypes and abnormal motile cilia structure, albeit the function of CFAP300 is not fully understood [89–95]. We here demonstrate that CFAP300 is a suitable marker for primary cilia across multiple human tissues. For example, the antibody targeting CFAP300 shows a specific staining in immunohistochemical (IHC) DAB stainings in the fallopian tube (motile cilia), the kidney (primary cilia), the thyroid gland (primary cilia), the liver (primary cilia of cholangiocytes), or the cervix (primary cilia) (Fig. 5B). Immunofluorescence (IF) co-staining with ARL13B and PCNT show that CFAP300 clearly marks primary cilia in the kidney, the thyroid gland, the cerebellum, the cortex, the adrenal gland, the salivary gland, the breast, the cervix, the liver (cholangiocyte cilia), the pancreas, the smooth muscle, and the colon, where mesenchymal cells are ciliated (Fig. 5C). We suggest CFAP300 to be a new reliable cilia marker, complementary to the existing commonly applied marker panel.

Revealing diseases with ciliary defects

To evaluate the functional significance of the newly identified ciliary proteins and to uncover potential clinically relevant ciliopathy genes, we compared the 654 proteins detected in primary cilium (including tip and transition zone) or basal bodies with phenotype annotations in the Online Mendelian Inheritance in Man (OMIM) database [96]. This analysis resulted in three distinct groups: (1) Genes found in OMIM with a known phenotype (n=300), (2) Genes found in OMIM without an associated phenotype (n=307) and (3) Genes not listed in OMIM (n=47) (Supplementary Table 10, Fig. 6A). Most genes (197 of 300 in group 1, 303 of 307 in group 2, and 46 of 47 in group 3) were not labeled as ciliopathy-causing genes in OMIM (Fig. 6A).

We convolved the clinical analysis of the protein list with the newly discovered proteins that had not been related to cilia before, resulting in the identification of 13 highly interesting proteins with potential disease associations but without described cilia- or ciliopathy-relationships, for which we now provide evidence of localization to cilia (Fig. 6A). Most of these showed a high spatiotemporal variation across cilia, and surprisingly, many of these proteins are enriched in the brain tissue or fulfill key roles in neurons. These include: the cell adhesion molecule NRCAM (Fig. 6B), which is involved in cell-cell contacts and axon outgrowth in the peripheral- and central nerve system [97]; the aromatic-L-amino-acid decarboxylase DDC (Fig. 6B) involved in neurotransmitter metabolism; the Neuronal tyrosine-phosphorylated phosphoinositide-3-kinase adapter 2 NYAP2 (Fig. 6B), which belongs to a family of proteins that regulates neuronal morphogenesis [98]; The calcium/calmodulin-dependent kinase CAMK1G (Fig. 3B), which can act in a calcium/calmodulin

dependent signaling cascade important for axon formation [99]; the calcium/calmodulin dependent protein kinase II inhibitor 1 CAMK2N1 (Fig. 6B), which inhibits CAMK2, a key kinase in many neuronal functions [100]. Furthermore, we identified the E3 ubiquitin ligase ZNRF1 at the transition zone (Fig. 6B) - ZNRF1 is enriched in the nervous system and targets various receptors [101], but also interacts with tubulin [102]. The little studied actin binding transcription modulator ABITRAM was observed in individual cilia of ASC52telo and hTERT-RPE1 (Fig. 6B). We found the GPCR LPAR3 in individual cilia, as described above (Fig. 4F). Interestingly, LPA signaling has recently gained more attention in ciliogenesis regulation and glioblastoma, yet focusing on LPA detection through LPAR1 but lacking clarity on where endogenous LPARs localize [103–105]. Furthermore, in a study using zebrafish as a model organism, LPAR3 had been recently implicated to be crucial for establishing Left-Right asymmetry [106], where cilia are known to play important roles, and brain functions [107]. Exogenous FLAG-tagged LPAR1 and LPAR3, introduced by overexpression, have been shown to localize to cilia of immortalized astrocytes [104]. We now reveal endogeneous LPAR3 in human cilia, supporting the relevance for LPA signaling in cilia and emphasizing that LPA signaling may occur through the cilium. An additional protein that we revealed in cilia is AXIN1 (Fig. 6B), reported to be part of the beta-catenin destruction complex and to regulate beta-catenin levels and modulate Wnt signaling [108–110]. Just recently, Wnt signaling has been highlighted as an additional signaling pathway in primary cilia [111]. We add AXIN1 to the picture of the Wnt signaling pathway in cilia. Interestingly, those cilia showing AXIN1 staining in hTERT-RPE1 cells were off focus compared to the cell nucleus, sticking into the liquid space of the culture well (Fig. 6B). Furthermore, we revealed in cilia the kinesin KIF26B (Fig. 6B), the calcium-dependent regulator of potassium channels ANO3 (Fig. 6B), and the uncharacterized proteins RUNDC3B (Fig. 6B), and ANKRD65 (Fig. 6B).

Lastly, we investigated genes from groups two and three (Fig. 6A) in clinical samples analyzed at the Karolinska University Hospital by whole genome sequencing (WGS) [112,113]. Clinical WGS data from three patient groups were analyzed: 1) patients with suspected ciliopathy without a causative variant found (n=157), 2) fetuses with an ultrasound-detected malformation without a causative variant found (n= 470) and 3) patients who had undergone a clinical patient-parental trio WGS analysis (n= over 1,500). We searched for potential clinically relevant single nucleotide variants in the 354 genes in groups two and three (Fig. 6A, Supplementary Table 10) in the WGS data from these three patient groups by one gene at a time, filtering for frameshift variants, nonsense variants and predicted splicing variants in homozygous, compound heterozygous or *de novo* states. Interestingly, we identified one individual in the trio cohort for whom a *de novo* two nucleotide deletion was detected in *CREB3* (NM_006368) (c.810_811del/p.Ser271*) causing a premature stop codon. The individual was a young boy with blindness due to optical nerve hypoplasia. His other symptoms include retinal changes, nystagmus, low bone density, short stature and hypoglycemia. We observed CREB3 in the cilia of RPTEC/TERT1 cells with an enrichment at the ciliary tip, at the transition zone region in ASC52telo cells, and at basal bodies or the transition zone, or at the tip in starved hTERT-RPE1 cells (Fig. 6C). This pattern of localization to the ciliary base and tip might indicate that CREB3 shuttles through primary cilia. As ciliopathies are rare disorders, patients are often diagnosed after months to years only, or the disease ontogeny remains unresolved since the disease-causing genetic variants are not located in known ciliopathy genes. As we demonstrate here, our new dataset provides new avenues for

clinics to reveal potential new ciliopathies and better understand ciliopathies by showing where cilium related proteins localize.

Discussion

Our study provides the first insight into single-cilia proteomic heterogeneity and a unique resource for the cilia community to develop new hypotheses about the cellular functions governed by the primary cilium and their underlying mechanisms. We resolve domains of heterogeneity, i.e., within and across cell populations, highlight the specificity of ciliary signaling pathways, reveal ciliary microdomains, identify a new ciliary marker, and employ our atlas to unlock the mystery behind unresolved ciliopathy-like cases.

The composition of primary cilia has been studied systematically by proximity-labeling based MS-proteomics approaches, which have provided lists of proteins to localize to cilia of a few murine and human cell types [20–23]. Yet, such approaches require pooling millions of cilia into one measurement and contrasting the measurements of ciliary and other cell compartments to reach subcellular specificity, which in turn renders the detection of multilocalizing proteins that are less abundant in the cilium than in the cytoplasm impossible. Consequently, we lack a systemic understanding of diversity of the ciliary proteome among individual cilia, and of proteins that are multilocalizing to cilia and other cell compartments. Furthermore, comparative studies on the ciliary proteome so far reside on phylogenetic studies or comparison across species [24,39]. Comparing multiple human cell types has not been realized, which might be due to the limitation of proximity-labeling-approaches not being functional in many cell types. In turn, the studies on the cell-specificity of ciliary proteins have focused on a few proteins. For example, many years of mechanistic research, using genetic tools, cellular models, and model organisms have established that GPCRs localize to cilia with cell-type specificity [114]. With our method we greatly advance the understanding of cilia as we show that a broad variety of ciliary proteins, not only receptors but also kinases like PI3K, AKT kinases, or calmodulin-dependent kinases, as well as Cytoskeleton-related proteins, i.e., Septins, and enzymes are in fact cell-type- and even single-cell-specifically localized to the cilium. Importantly, we observe that proteins - when not localizing to cilia - are still expressed and localized to other cell compartments. We show that 99% of the investigated ciliary proteins multilocalize and that when a protein is not localizing to cilia it appears in other cellular structures. We thereby highlight that ciliary specificity across cell types is substantially driven by protein trafficking rather than gene expression. Ciliary import and export have been identified as a signal transduction mechanism, such as in Hedgehog signaling [1]. We demonstrate that many more signaling pathways are underlying spatiotemporal ciliary dynamics and propose that cells rapidly fine-tune their antenna to individually sense their environment depending on their specific task in a cellular consortium. The fact that we also observe downstream signaling machinery in cilia, such as kinases like AKTs, further stresses that the cilium is not just a cellular antenna but also a computer that integrates signals to compute a response decision, to be relayed to the cell body. This concept has been well established for sperm cells before, where local signaling machinery in the flagellum modifies the flagellar beating for steering the cell [115] - our data indicates that this concept holds true for cilia as well.

Structurally, we go beyond the resolution of previous studies and provide the localization of proteins to cilia with the resolution of confocal microscopy. This is the first proteomic study that distinguishes the protein composition of tip, cilium, transition zone, and basal bodies in the same cells. We thereby demonstrate that the different ciliary regions may be specifically functionalized for different aspects of signaling, which may be modes of shaping the computational architecture of the cilium. Of note, our results hint at spatiotemporal organization beyond the compartments commonly known and that we annotated (Cilium, Tip, Transition zone, Basal Body). We conclude that the ciliary protein architecture is spatially highly organized into microdomains, which are likely dynamic. Our data set can serve as a starting point for systematic super-resolved cilia studies, for example using expansion microscopy or cryo-CLEM.

Importantly, the ciliary compartment is not just organized on the level of proteins. Beyond signaling molecules, we also reveal enzymes in cilia that may close gaps in our understanding of how the ciliary compartment is organized. For example, we reveal an enzyme involved in sterol synthesis supporting the hypothesis that cilia locally metabolize their unique lipid environment for customizing or conducting signaling pathways [73]. The presence of the other enzymes indicates that the cilium has its own metabolism, which may be crucial to further study to understand its contribution to ciliary signaling pathways and functions. The heterogeneity in these factors highlights the importance for single-cell spatially-resolved methods for protein, lipid, and metabolite measurements to further delineate the complex architecture of the ciliary compartment.

Beyond revealing the cilium as a signaling device, our data also highlights new avenues for cilia research. For example, we surprisingly detect the least number of cell-type-unique proteins in ASC52telo cells, which show only 16 or 12 cell-type unique primary cilia or basal body protein localizations - much less than hTERT-RPE1 (68 or 73, respectively) or RPTEC/TERT1 cells (69 or 62, respectively). We cannot exclude that a technical limitation hampered discovery in ASC52telo cells: they have shorter cilia compared to the other two cell types (Fig. 1D), which typically lie flat on the cells, and they show a significantly lower ciliation rate. However, the fraction of proteins not previously described for cilia in our candidate list was collected with a strong focus on signaling cascades. Based on our gene ontology analysis of ASC52telo cells and the fact that they have cilia only for a very short time due to their fast cell cycle, we hypothesize that the cilium of ASC52telo cells is less tuned to receptor-based signaling but rather crucial for driving stemness and asymmetric cell division in a stem-cell population. Such asymmetry may be produced by the ASC52telo cells retaining a ciliary vesicle or whole cilium during cell division. Thus, our data encourage us to next direct our antibody-based spatial proteomics methods to stem cells with an expanded candidate gene list tailored to stem cell functions. Furthermore, we surprisingly identified many neuron- and brain-related proteins in cilia, which emphasizes that our focus should also direct towards neuronal cilia. Of note, some of these proteins relate to synapses or axons, supporting the recent observations of the cilium being involved in synaptic transmission [63] and that the cilium is not just an organelle that is a free-floating antenna but that can also establish contacts with other structures, i.e., synapses, for even more local signal reception.

Our study opens up many new avenues for ciliary research. First of all, we have tested and validated antibodies for 654 proteins in primary cilia in human cells. Most of these antibodies are

commercially available and allow the field to probe ciliary signaling and structure in detail, for example, when investigating patient-derived cells to explore disease mechanisms. Second, we also show that our screen has the potential to be translated to deep studies of human tissues, which we pursued for revealing CFAP300 as a new ciliary marker. Notably, many of the other antibodies that we tested are also suitable for tissues, as they are already validated in IHC workflows in the Human Protein Atlas [25,32]. Recently, we also showed that the antibody for ATF3, which we identified at the Basal Body, is also applicable to study the role of cilia in the developing human heart [116]. Third, we generate the basis for revealing additional ciliopathy cases in the clinics. We demonstrate that our new atlas can link a clinical phenotype of a CREB3 variant to the cilium.

In summary, we highlight the primary cilium as a cellular compartment with a diverse proteome involved in signal transduction mechanisms. The ciliary compartment is tightly regulated to bring together certain signaling molecules in time and space. We hypothesize that cells employ their cilia to customize sensation and signal transduction to individual cellular roles. Thereby, the primary cilium might be a space in which the cell can both tailor their environmental sensing abilities and customize the internal computation to allow precise cell type and state-tuned signaling. Our data indicates that there are multiple domains of ciliary heterogeneity potentially relating to cell states, such as cell cycle, ciliogenesis, signaling, and metabolism. Further deep analysis of our data set followed up by functional assays and live measurements of the proteins undergoing heterogeneity, will allow the cilia community to further define these axes of heterogeneity. Hence, this study serves as a starting point for cilia systems biology, providing a template for modeling the cilium as an information processing unit. With all our data being publicly explorable at https://www.proteinatlas.org we pave new avenues for research on decoding the fundamental biology of human primary cilia and clinical implications such as in ciliopathies.

Figures

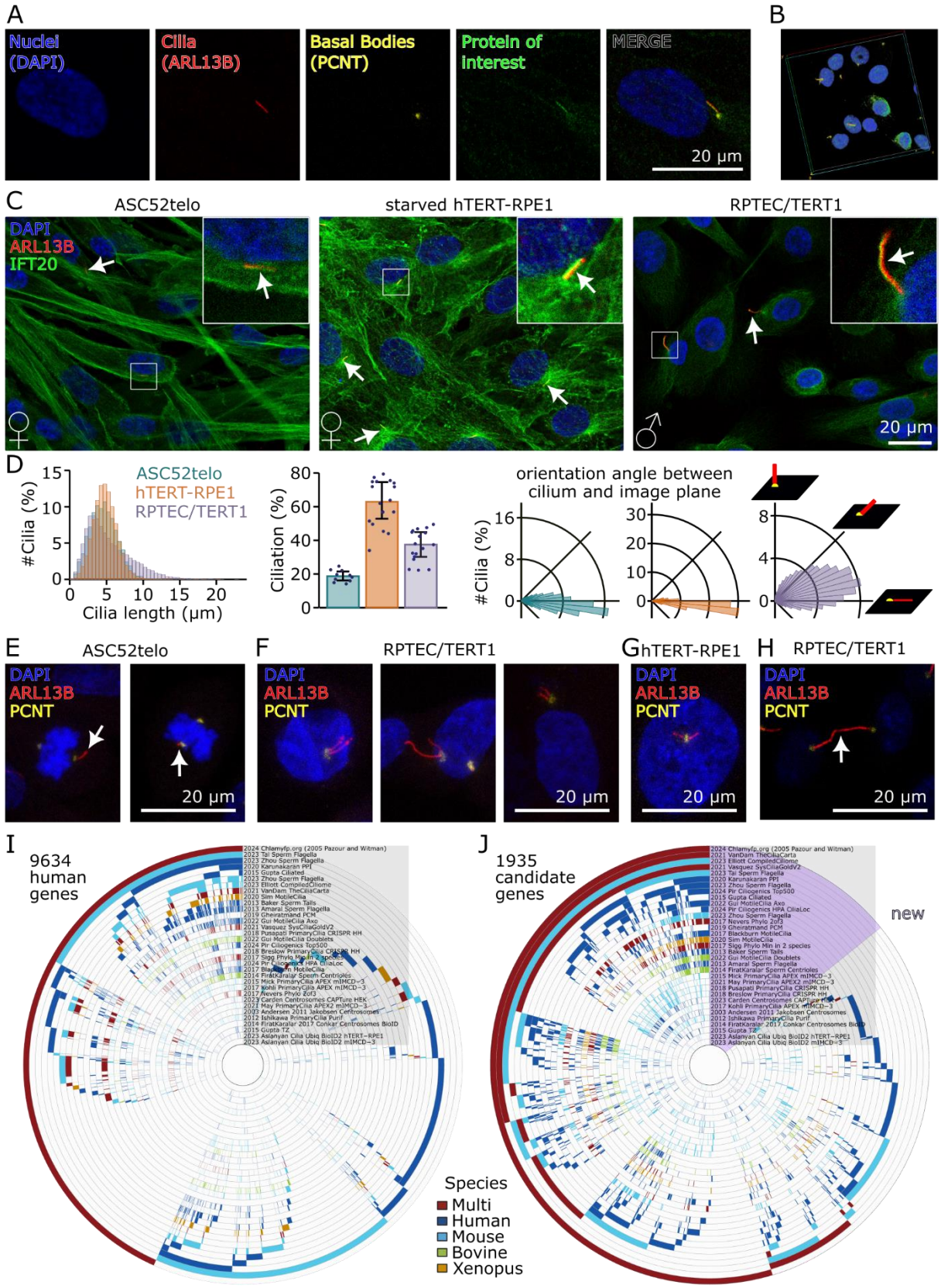
A
Nuclei (DAPI)
Cilia (ARL13B)
Basal Bodies (PCNT)
Protein of interest
MERGE
20 µm
B
C
ASC52telo
starved hTERT-RPE1
RPTEC/TERT1
DAPI
ARL13B
IFT20
20 µm
D
ASC52telo
hTERT-RPE1
RPTEC/TERT1
#Cilia (%)
Cilia length (µm)
Ciliation (%)
orientation angle between cilium and image plane
E
ASC52telo
F
RPTEC/TERT1
G
hTERT-RPE1
H
RPTEC/TERT1
DAPI
ARL13B
PCNT
20 µm
I
9634 human genes
J
1935 candidate genes
new
Species
Multi
Human
Mouse
Bovine
Xenopus

Figure 1: Spatially profiling the primary cilia proteome

A-B) New staining concept. **A)** Ciliated cells (i.e., starved hTERT-RPE1) cells are co-stained with markers for nuclei (DAPI), cilia (ARL13B antibody), basal bodies (PCNT antibody) and for a protein of interest (i.e., with a polyclonal antibody against IFT43 from the Human Protein Atlas). **B)** Confocal z-stacks are generated, which allow 3D analysis of the whole cell including the cilia, even when they stick out of the cell to the top or bottom (Blue: Nuclei, Red: Cilia, Yellow: Basal Body, Green: Protein of Interest). **C)** Three cell lines are investigated: ASC52telo cells from the adipose tissue, starved hTERT-RPE1 cells from the retina, and RPTEC/TERT1 cells from the kidney. Example images from all three cell lines are shown with magnified insets, from a co-staining of DAPI (labeling nuclei), ARL13B (labeling cilia), and the protein of interest IFT20. Gender of the cell line indicated. **D)** CiliaQ analysis of all images underlying this study reveals the cilia length distribution, ciliation rate, and ciliary orientation angle. Percentages of cilia refer to the total number of cilia by cell line. In total, 236,504 cells with 110,844 cilia were included. Left plot: Normalized histograms of the cilia lengths for all cilia analyzed, distinguished by cell line. Middle plot: Each dot represents all images from one individual experiment day. Bars and error bars represent median and quantiles, respectively. Right plot: Radial histograms of the ciliary orientation angles for all cilia analyzed. The orientation angle was determined as the angle between the vectors from the basal body center to the ciliary tip and the image plane. **E-H)** Example images of special cilia observations in the three different cell lines. Only the Nucleus (DAPI), cilia (ARL13B), and Basal Body (PCNT) channels are displayed. **E)** Mitotic ASC52telo cells retaining a cilium. **F)** RPTEC/TERT1 cells with two adjacent cilia. **G)** Starved hTERT-RPE1 cell with two adjacent cilia. **H)** Two adjacent RPTEC/TERT1 cells whose cilia are connected and form a “bridge”. **I)** Sunburst plot of all data sets accumulated to form the cilia candidate list of 9634 human genes. Different data sets and studies, as well as additional educated guesses were convolved (see Materials & Methods). Each study is colored by species. **J)** Candidate list of 1,935 genes for which a staining with Human Protein Atlas antibodies was conducted, including a substantial portion of genes that had not been associated with cilia before (“new”, purple). Scale bars indicated.

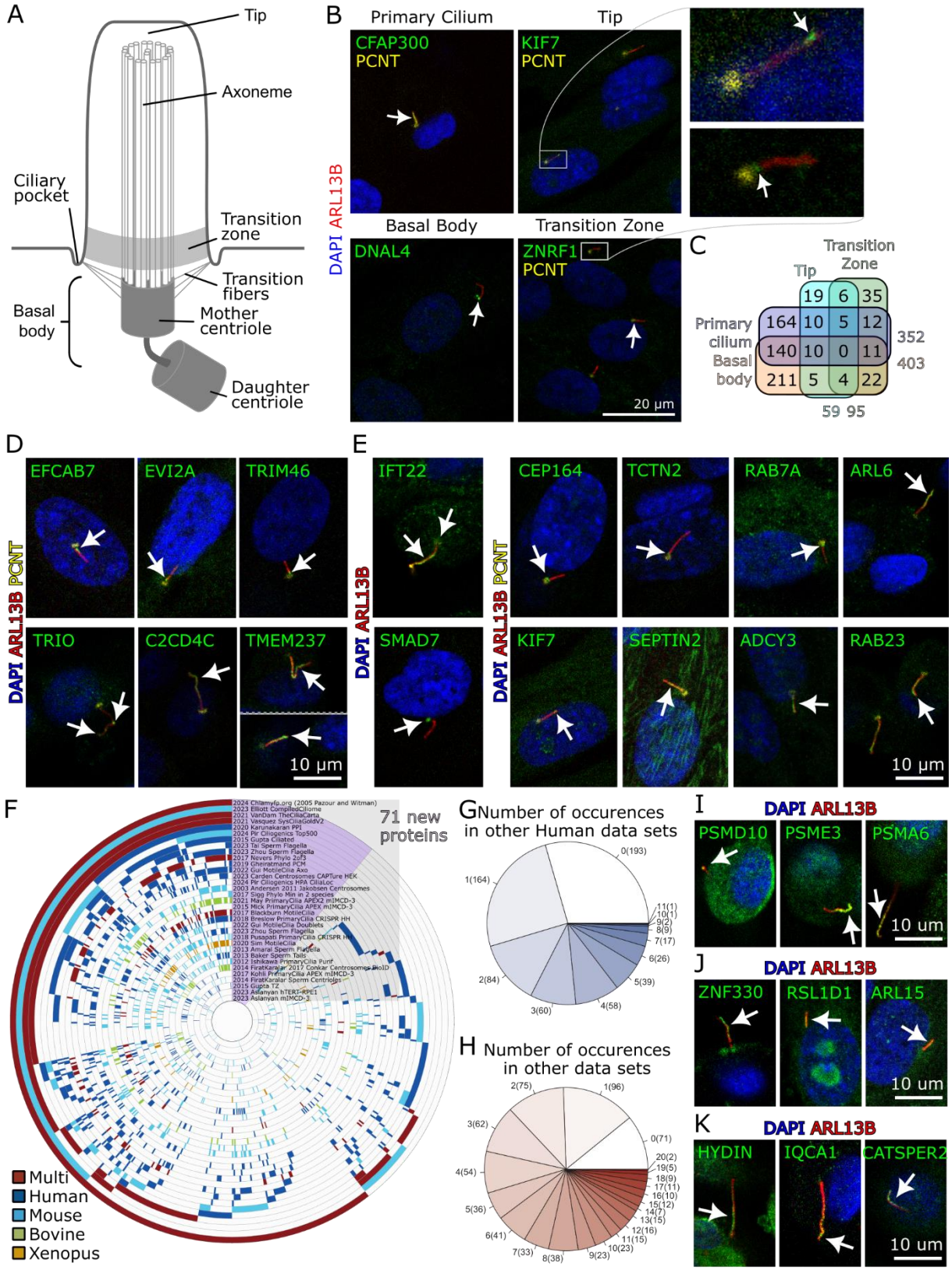
A
Tip
Axoneme
Ciliary pocket
Transition zone
Transition fibers
Basal body
Mother centriole
Daughter centriole
B
Primary Cilium
Tip
CFAP300
PCNT
KIF7
PCNT
DAPI ARL13B
Basal Body
Transition Zone
DNAL4
ZNRF1
PCNT
20 µm
C
Transition Zone
Tip
Primary cilium
Basal body
19 6 35
164 10 5 12
140 10 0 11
211 5 4 22
352
403
59 95
D
EFCAB7
EVI2A
TRIM46
DAPI ARL13B PCNT
TRIO
C2CD4C
TMEM237
10 µm
E
IFT22
CEP164
TCTN2
RAB7A
ARL6
DAPI ARL13B PCNT
SMAD7
KIF7
SEPTIN2
ADCY3
RAB23
10 µm
F
71 new proteins
Multi
Human
Mouse
Bovine
Xenopus
G Number of occurences in other Human data sets
0(193)
1(164)
2(84)
3(60)
4(58)
5(39)
6(26)
7(17)
8(9)
9(2)
10(1)
11(1)
H Number of occurences in other data sets
0(71)
1(96)
2(75)
3(62)
4(54)
5(36)
6(41)
7(33)
8(38)
9(23)
10(23)
11(15)
12(16)
13(15)
14(7)
15(12)
16(10)
17(11)
18(9)
19(5)
20(2)
I
DAPI ARL13B
PSMD10
PSME3
PSMA6
10 um
J
DAPI ARL13B
ZNF330
RSL1D1
ARL15
10 um
K
DAPI ARL13B
HYDIN
IQCA1
CATSPER2
10 um

Figure 2: Spatial map of the primary cilia proteome

A) Schematic drawing of a primary cilium and its substructures. **B)** Protein localization to four ciliary substructures was annotated, for which example images are shown: Primary cilium, if the protein was overlapping with the ciliary marker ARL13B; Primary cilium Tip (Tip), if the protein of interest channel showed a signal at the distal end of the cilium; Basal Body, if the protein of interest channel showed signals overlapping or accumulating close to the basal body marker PCNT; Primary cilium transition zone (Transition zone) if the protein of interest channel showed an enrichment between basal body and cilium. **C)** Venn diagram showing the number of genes observed at one or multiple of the four locations specified in B. **D)** Example images (single confocal slice images) of additional subpatterns observed in primary cilia. Gray interrupted line distinguishes two individual images placed adjacently for showing two cilia. **E)** Example images (single confocal slice images) of stainings for proteins that are established as localizing to cilia - gene names are shown. **F)** Comparing the list of genes encoding proteins that were annotated as localizing to at least one of the four cilium locations (B) to existing datasets. 71 proteins were not found in other datasets. **G-H)** Pie charts showing the number of occurrences in other datasets for each gene that encoded a protein found in one of the four annotated cilia compartments. **G)** Comparing the list of revealed proteins to datasets derived from Human samples only. **H)** Comparing the list of revealed proteins to datasets from any species. **I)** Example images of proteasomal subunits observed in cilia. **J)** Example images (single confocal slice images) for proteins observed in cilia that were previously only detected in individual proximity-labeling-based MS approaches. **K)** Motile cilia proteins detected in the cilia of RPTEC/TERT1 cells. Images were derived from stainings of different cell lines: Starved hTERT-RPE1 cells: DNAL4, ZNRF1, EFCAB7, EVI2A, TRIM46, SMAD7, RAB7A, SEPTIN2, RAB23, ARL15; RPTEC/TERT1 cells: CFAP300, TRIO, C2CD4C, TMEM237, IFT22, ARL6, PSMD10, PSME3, PSMA6, HYDIN, IQCA1, CATSPER2; ASC52telo cells: KIF7, CEP164, TCTN2, KIF7, ADCY3, ZNF330, RSL1D1.

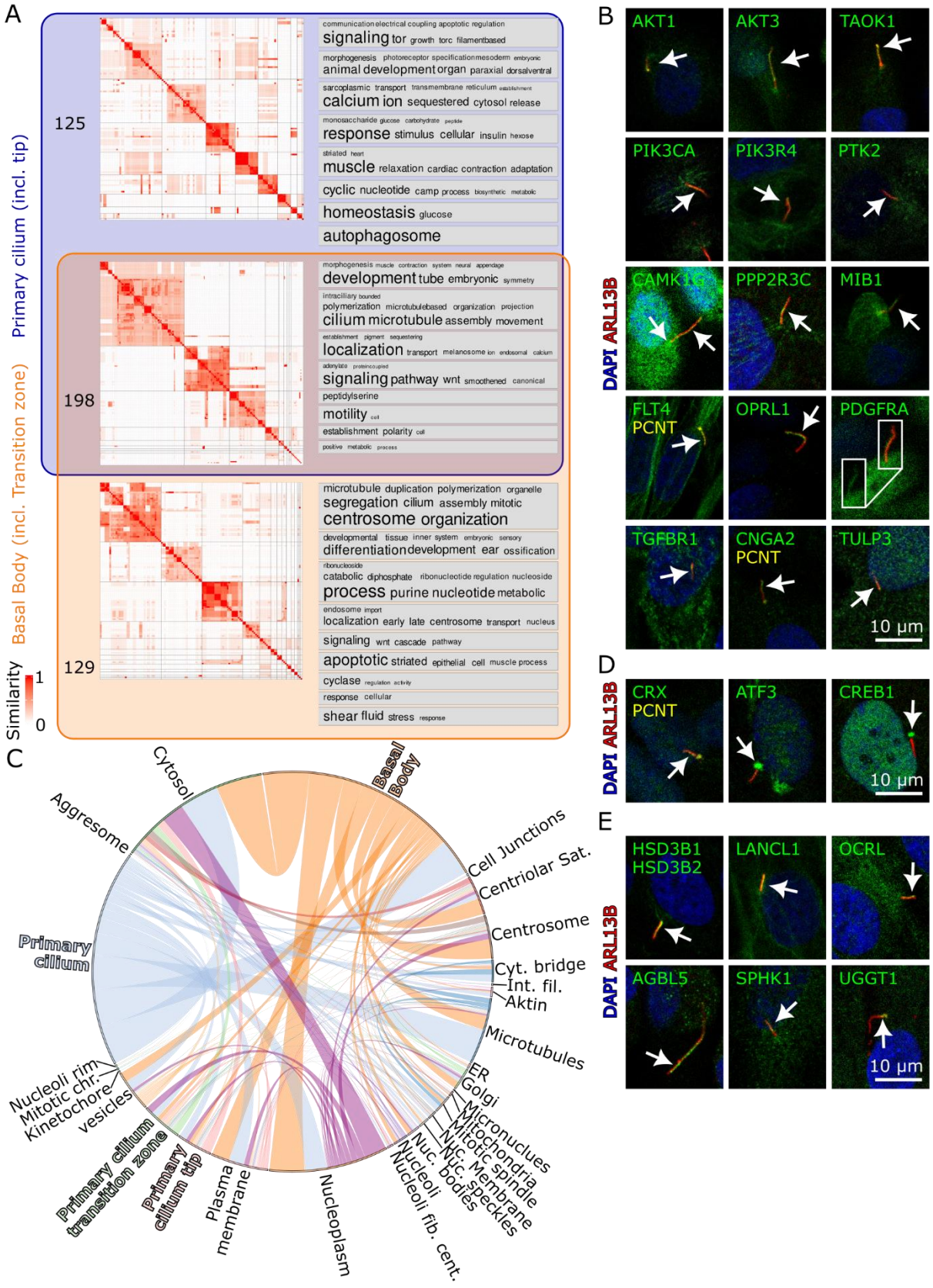
A
Primary cilium (incl. tip)
Basal Body (incl. Transition zone)
125
198
129
Similarity
1
0
signaling tor growth torc filamentbased
animal development organ paraxial dorsalventral
calcium ion sequestered cytosol release
response stimulus cellular insulin hexose
muscle relaxation cardiac contraction adaptation
cyclic nucleotide camp process
homeostasis glucose
autophagosome
development tube embryonic
cilium microtubule assembly movement
localization transport melanosome
signaling pathway wnt smoothened canonical
peptidylserine
motility
establishment polarity
centrosome organization
differentiation development ear ossification
process purine nucleotide metabolic
localization early late centrosome transport nucleus
signaling wnt cascade pathway
apoptotic striated epithelial cell muscle process
cyclase
response cellular
shear fluid stress
B
AKT1
AKT3
TAOK1
PIK3CA
PIK3R4
PTK2
CAMK1G
PPP2R3C
MIB1
FLT4
PCNT
OPRL1
PDGFRA
TGFBR1
CNGA2
PCNT
TULP3
DAPI ARL13B
10 µm
C
Cytosol
Basal Body
Aggresome
Cell Junctions
Centriolar Sat.
Centrosome
Primary cilium
Cyt. bridge
Int. fil.
Aktin
Microtubules
ER
Golgi
Micronuclues
Mitochondria
Mitotic spindle
Nuc. Membrane
Nuc. speckles
Nucleoli
Nuc. bodies
Nucleoli fib. cent.
Nucleoplasm
Plasma membrane
Primary cilium tip
Primary cilium transition zone
Nucleoli rim
Mitotic chr.
Kinetochore
vesicles
D
CRX
PCNT
ATF3
CREB1
DAPI ARL13B
10 µm
E
HSD3B1
HSD3B2
LANCL1
OCRL
AGBL5
SPHK1
UGGT1
DAPI ARL13B
10 µm

Figure 3: The primary cilium is a signaling hub

A) Comparative Gene Ontology enrichment analysis of Biological Process terms between the two major cilia locations primary cilium (including tip) and basal body (including transition zone). The Venn diagram shows the number of terms found to be significantly enriched (adj. P value < 0.01 and q value < 0.01) for only primary cilium (n=125) or basal body (n=129), as well as for both locations (n=198). Significant terms were clustered by semantic similarity, and for each resulting GO term cluster, a word cloud is shown summarizing the biological functions of the terms in the cluster based on keywords enrichment of term names. The font size in the word clouds correlates with -log(P value) of the key word enrichment, i.e. the larger, the more enriched a keyword is compared against background GO vocabulary. The color in the heat maps represents the semantic similarity. **B)** Protein localization of example signaling proteins to the primary cilium. All images show single confocal slice images except for PDGFRA, where a maximum intensity projection of 5 confocal slices is shown to show the whole cilium. The inset for PDGFRA shows the same position with displaying only the PDGFRA channel. **C)** Multilocalization of cilia-related proteins with the other 35 annotated subcellular compartments. Abbreviations: Centriolar Sat. = Centriolar Satellites; Cyt. bridge = cytokinetic bridge; Int. Fil. = Intermediate Filaments; Mitotic chr. = Mitotic chromosome; Nuc. bodies = Nuclear bodies; Nucleoli fib. cent. = Nucleoli fibrillar center; Nuc. Membrane = Nuclear membrane; Nuc. speckles = Nuclear speckles. **D)** Example transcription factors revealed in cilium and nucleus. **E)** Example enzymes revealed in cilia. Images were derived from stainings of different cell lines: Starved hTERT-RPE1 cells: PTK2, PP2R3C, CNGA2, TULP3, CRX, ATF3, CREB1, HSD3B1/HSD3B2, LANCL1, OCRL, SPK1; RPTEC/TERT1 cells: AKT1, AKT3, TAOK1, PIK3CA, PIK3R4, CAMK1G, MIB1, OPRL1, PDGFRA, AGBL5, UGGT1; ASC52telo cells: FLT4, TGFBR1.

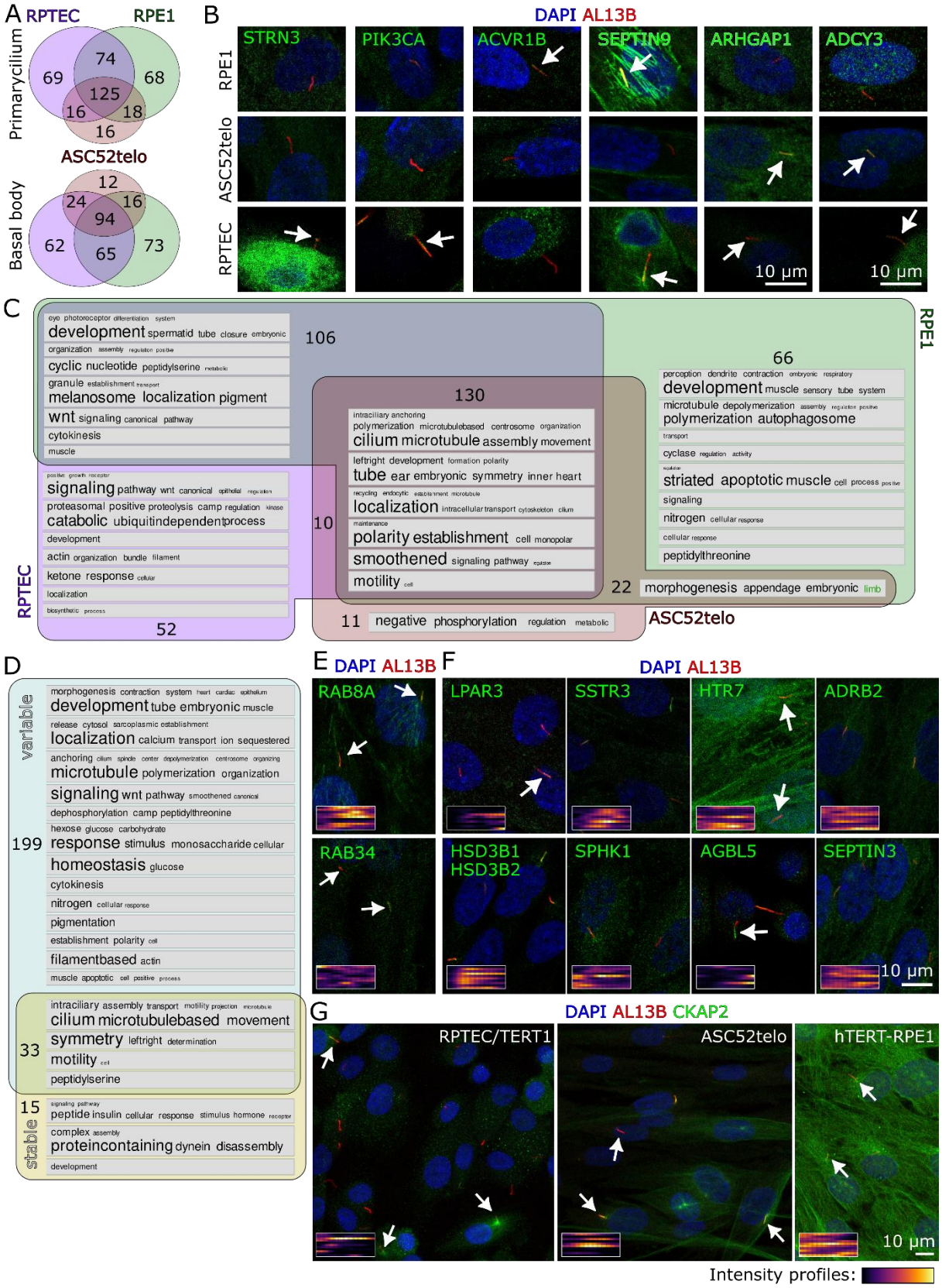
A
RPTEC
RPE1
Primarycilium
74
69
68
125
16
18
16
ASC52telo
Basal body
12
24
16
94
62
65
73
B
DAPI AL13B
RPE1
ASC52telo
RPTEC
STRN3
PIK3CA
ACVR1B
SEPTIN9
ARHGAP1
ADCY3
10 µm
10 µm
C
RPE1
RPTEC
ASC52telo
106
130
66
10
52
22
11
development spermatid tube closure embryonic
organization assembly regulation positive
cyclic nucleotide peptidylserine metabolic
granule establishment transport
melanosome localization pigment
wnt signaling canonical pathway
cytokinesis
muscle
signaling pathway wnt canonical epithelial regulation
proteasomal positive proteolysis camp regulation kinase
catabolic ubiquitindependentprocess
development
actin organization bundle filament
ketone response cellular
localization
biosynthetic process
intraciliary anchoring
polymerization microtubulebased centrosome organization
cilium microtubule assembly movement
leftright development formation polarity
tube ear embryonic symmetry inner heart
recycling endocytic establishment microtubule
localization intracellular transport cytoskeleton cilium
maintenance
polarity establishment cell monopolar
smoothened signaling pathway regulation
motility cell
perception dendrite contraction embryonic respiratory
development muscle sensory tube system
microtubule depolymerization assembly regulation positive
polymerization autophagosome
transport
cyclase regulation activity
striated apoptotic muscle cell process positive
signaling
nitrogen cellular response
cellular response
peptidylthreonine
morphogenesis appendage embryonic limb
negative phosphorylation regulation metabolic
D
variable
stable
199
33
15
morphogenesis contraction system heart cardiac epithelium
development tube embryonic muscle
release cytosol sarcoplasmic establishment
localization calcium transport ion sequestered
anchoring cilium spindle center depolymerization centrosome organizing
microtubule polymerization organization
signaling wnt pathway smoothened canonical
dephosphorylation camp peptidylthreonine
hexose glucose carbohydrate
response stimulus monosaccharide cellular
homeostasis glucose
cytokinesis
nitrogen cellular response
pigmentation
establishment polarity cell
filamentbased actin
muscle apoptotic cell positive process
intraciliary assembly transport motility projection microtubule
cilium microtubulebased movement
symmetry leftright determination
motility cell
peptidylserine
signaling pathway
peptide insulin cellular response stimulus hormone receptor
complex assembly
proteincontaining dynein disassembly
development
E
DAPI AL13B
RAB8A
RAB34
F
DAPI AL13B
LPAR3
SSTR3
HTR7
ADRB2
HSD3B1
HSD3B2
SPHK1
AGBL5
SEPTIN3
10 µm
G
DAPI AL13B CKAP2
RPTEC/TERT1
ASC52telo
hTERT-RPE1
10 µm
Intensity profiles:

Figure 4: Cellular diversity and spatiotemporal dynamics of the primary cilia proteome

A) Venn diagram of the genes for the proteins identified in primary cilia (including tip and transition zone), distinguishing by cell line. Only genes included for which an approved staining was obtained from all three cell lines. (Abbreviations: RPTEC = RPTEC/TERT1, RPE1 = starved hTERT-RPE1) **B)** Example images (single confocal slice images) for stainings across the three cell lines, showing heterogeneity in ciliary localization across cell types. **C)** Comparative Gene Ontology enrichment analysis of Biological Process terms between the three included cell lines to investigate cell-line differences and commonalities. The Venn diagram shows the overlap of significantly enriched terms (adj. P value < 0.01 and q value < 0.01) for each cell line. Significant terms of each section of the Venn diagram were clustered by semantic similarity, and for each resulting GO term cluster, a word cloud is shown summarizing the biological functions of the terms in the cluster based on keywords enrichment of term names. The font size in the word clouds correlates with -log(P value) of the key word enrichment, i.e. the larger, the more enriched a keyword is compared against background GO vocabulary. Heat maps displaying the semantic similarities are shown in Supplementary Fig. 3. **D)** Comparative Gene Ontology enrichment analysis of Biological Process terms between proteins annotated as displaying intensity variation in one of the four ciliary locations, and annotated as stable as described in C). Heat maps displaying the semantic similarities are shown in Supplementary Fig. 5. **E)** Example images (single confocal slice images) for stainings of the two ciliogenesis-related proteins RAB8A and RAB34. **F)** Example images (single confocal slice images) of stainings revealing proteins with heterogeneous localization to primary cilia. **G)** Example images (maximum intensity projections of whole stack) of CKAP2 staining in the three cell lines. Cell lines for images (if not indicated): Starved hTERT-RPE1 cells: LPAR3, SSTR3, HTR7, ADRB2, HSD3B1 HSD3B2, SPHK1, RAB8A, SEPTIN3; RPTEC/TERT1 cells: AGBL5; ASC52telo cells RAB34. Insets in E-G show the intensity profiles of the proteins of interest for 10 individual example cilia (each row represents one cilium) from the center of the basal body (left) to the tip (right), revealed by CiliaQ analysis (see Materials and Methods).

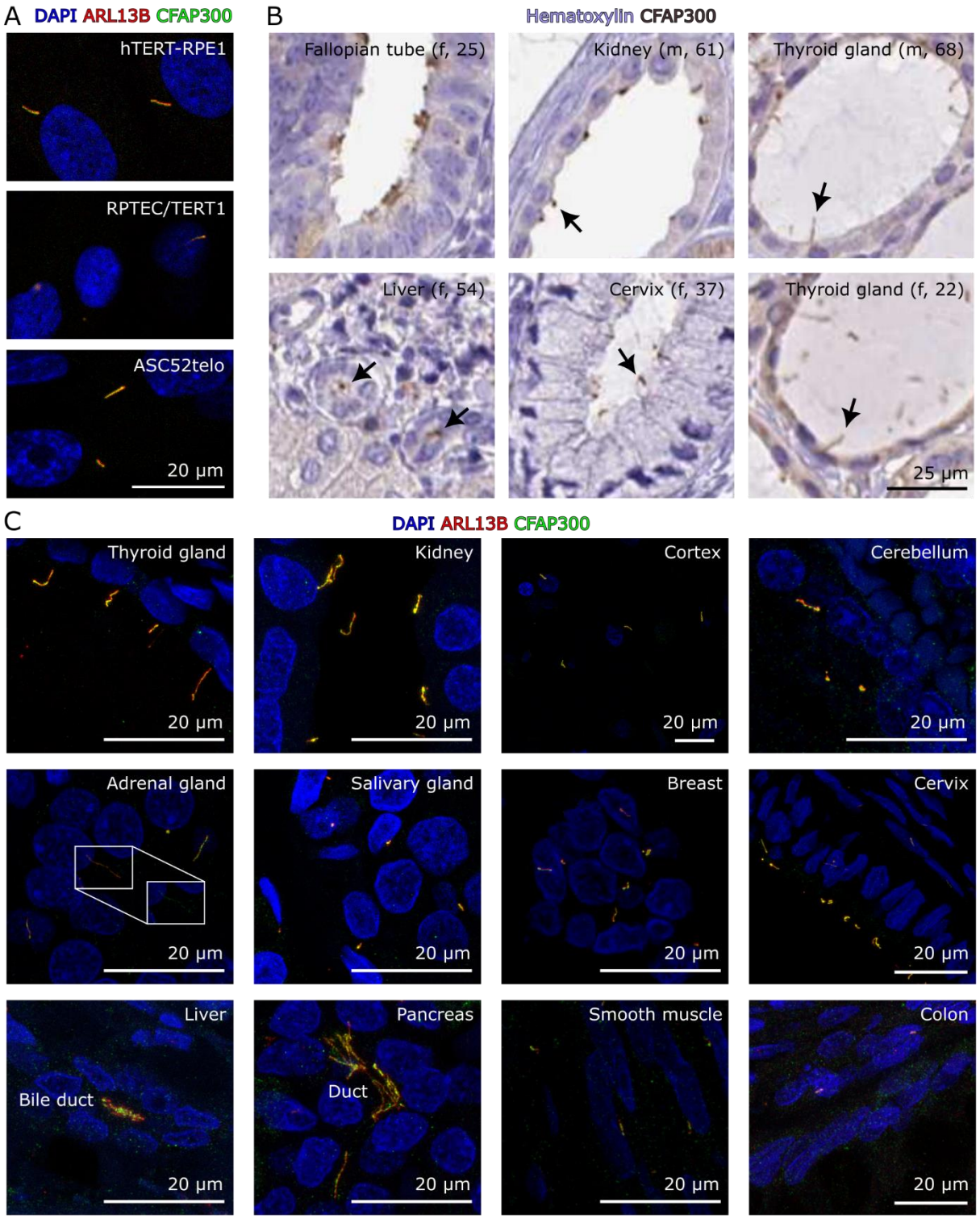

Figure 5: CFAP300 - a new ciliary marker protein

A) Example images for stainings of the CFAP300 in the three cell lines. **B)** Example images from IHC stainings on human tissues (sex and age indicated in brackets) with the CFAP300 antibody.

C) Confocal microscopy images (Maximum intensity projection of z-stack) from different human tissues stained with a CFAP300 antibody, cilia (ARL13B antibody), and nuclei (DAPI). Inset shows the indicated region again with only the DAPI and CFAP300 channel displayed.

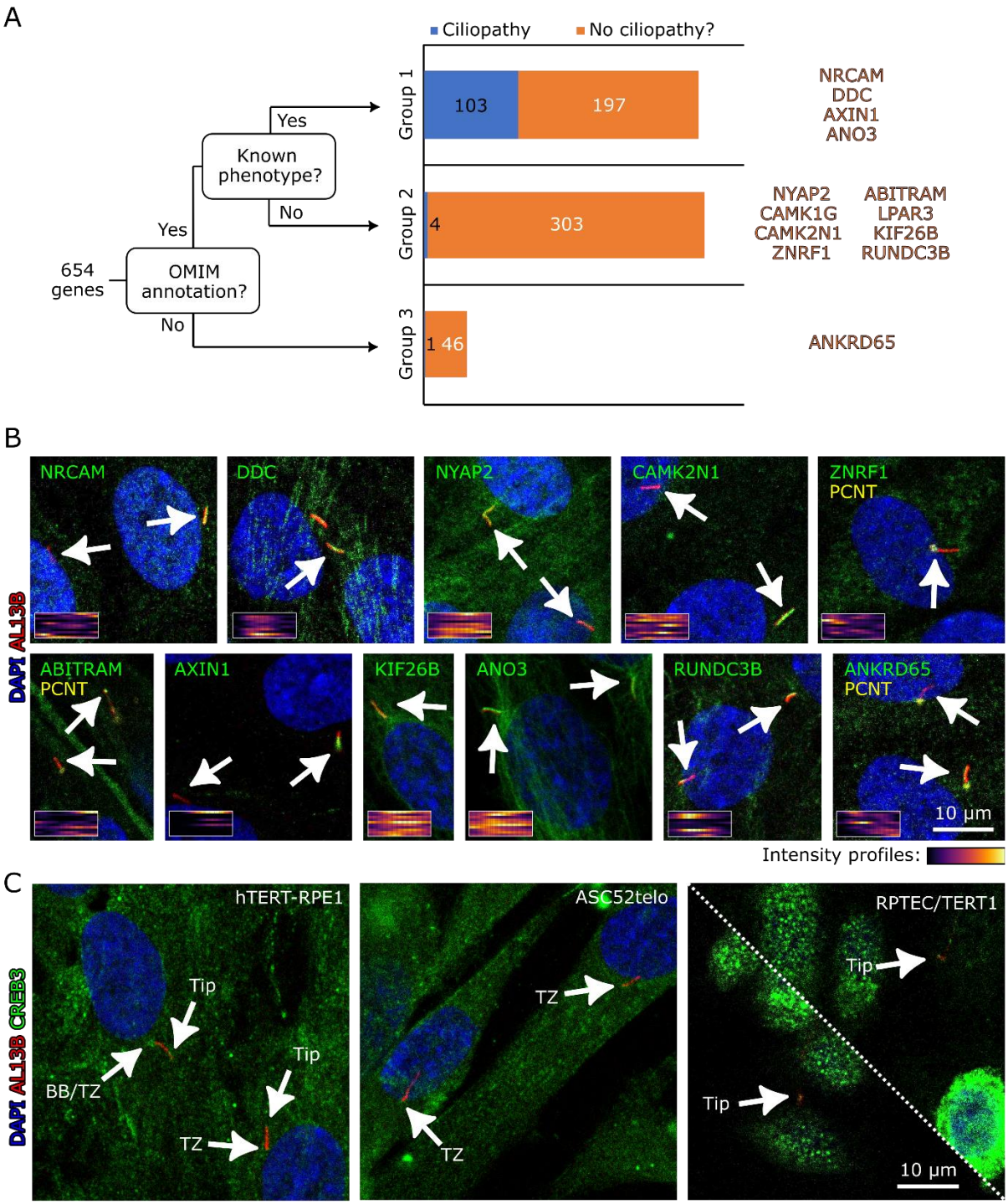

Figure 6: Clinical relevance of the newly revealed ciliary proteome

A) Flow chart for splitting the 654 genes into three groups based on their OMIM annotations. Additionally, the genes were classified by being established ciliopathy proteins. Example genes for each group are written on the right, and shown in B. **B)** Example images for staining the proteins for genes pointed out in A. Cell lines for images: Starved hTERT-RPE1 cells: NRCAM,

DDC, NYAP2, CAMK2N1, ZNRF1, AXIN1, KIF26B, ANO3; ASC52telo cells: ABITRAM. Insets show the intensity profiles of the protein of interest for 10 individual example cilia (each row represents one cilium) from the center of the basal body (left) to the tip (right), revealed by CiliaQ analysis (see Materials and Methods). **C)** Example images from stainings of CREB3 in hTERT-RPE1 cells (serum-starved), ASC52telo cells, or RPTEC/TERT1 cells. The white interrupted line distinguishes two images that were placed adjacently to show two cilia. Abbreviations: TZ = transition zone. BB = Basal Body. The basal body PCNT marker was not shown to better visualize the localizations of CREB3 - The PCNT marker was however used to correctly mark BB and TZ positions with arrows.

Materials and Methods

Developing a list of cilium-associated candidate proteins

Lists of genes or proteins detected in primary cilia, motile cilia, flagellum in humans and across other species were extracted from databases in the format of supplementary tables, PDF-files, or exportable csv files. The data from ChlamyFP.org (Human) were downloaded on July 10, 2024. The files were next imported into R and merged into a master list (Supplementary Table 1) by conversion of the protein or gene identifiers into Ensembl gene IDs using the R package biomaRt (version 2.56.1) [117]. Conversions failing in bioMart were converted - if possible - by automated queries to the Ensembl REST API (https://rest.ensembl.org). The data overlap was plotted using the library Plotrix (version 3.8.4). To reduce the list to the candidate list of 1,935 genes, we selected targets based on (1) whether the gene is expressed in the cell lines we aimed to study (using HPA internal cell line RNAsequencing data), (2) whether they represent gold standard cilia proteins, (3) whether the HPA antibody library provided a good, validated antibody for the protein of interest, and (4) the discovery potential of the protein of interest, with a strong focus on revealing signaling proteins in cilia.

Staining prioritization and order of experiments

We started by staining the one or two cell lines with highest RNA expression (HPA internal cell line RNA expression database) and did not pursue further staining in the other cell line(s) if the staining / antibody was deemed unspecific or unreliable or did not show cilium or basal body localization of the protein and in the other cell lines the protein was not indicated as expressed on RNA level. This resulted in not all proteins being stained in all three cell lines (Supplementary Fig. 10). For all conclusions drawn on inter-cell line diversity, only proteins that have been stained in all three cell lines were included.

Cell culture

hTERT-RPE1 cells (Evercyte GmbH, Vienna, Austria) were acquired from ATCC and cultivated in DMEM/F12 (Thermo Fisher Scientific Inc, GibcoTM, Cat. no. 11320033) + 10% FBS (Merck KGaA, Sigma-Aldrich, Cat. no. F7524) at 37°C and 5% CO2. ASC52telo and RPTEC/TERT1 cells were acquired from Evercyte GmbH (Vienna, Austria) and cultivated according to manufacturer's instructions. ASC52telo cells were cultivated in Endothelial Cell Growth Medium-2 (Lonza, Cat. no. CC-3162) supplemented with 4% FBS (Merck KGaA, Sigma-Aldrich, Cat. no. F7524) and 200 ug/ml G418 (G-418 Solution, Merck KGaA, Cat. no. 04727878001). RPTEC/TERT1 cells were cultivated in ProxUp2 medium (Evercyte, MHT-003-2).

Immunocytochemistry

Cells were seeded in 80 µl / well of the respective growth medium on 96-well glass-bottom plates (Greiner Sensoplate Plus, Greiner Bio-One, Germany) coated with 50 µl of 12.5 µg/ml human fibronectin (Sigma Aldrich, Darmstadt, Germany) and cultivated at 37 °C and 5% CO2. For hTERT-RPE1 and ASC52telo cells, approximately 10,000 cells/well were seeded. For

RPTEC/TERT1 cells, approximately 30,000 cells/well were seeded. hTRET-RPE1 cells were starved 24 hours after seeding by medium exchange to DMEM/F12 + 0.2% FBS, and fixed 48 hours after start of starvation. RPTEC/TERT1 cells were fixed 24 hours after seeding. ASC52telo cells were fixed 48 hours after seeding. For fixation, the cells were washed with phosphate-buffered saline (PBS, pH 7) and fixed with 40 µl 4% ice-cold paraformaldehyde (PFA: Sigma Aldrich, Darmstadt, Germany) dissolved in PBS for 15 min. Cells were washed with PBS and permeabilized with 40 µl 0.1% Triton X-100 (Sigma Aldrich) in PBS for 3 × 5 min. Rabbit polyclonal HPA antibodies targeting the proteins of interest were dissolved to 2–4 µg/ml in blocking buffer (PBS + 4% FBS) containing the cilia marker antibodies against ARL13B (Abcam, ab136648, mouse IgG2a, 1:2000) and PCNT (Abcam, ab28144, mouse IgG1, 1:2000). After washing with PBS, the diluted primary antibodies were added (40 µl per well), and the plates were incubated overnight at 4 °C. After overnight incubation, wells were washed with PBS for 3 × 10 min. Secondary antibodies, goat-anti-mouse-IgG1k-Cross-Adsorbed-Alexa555 (ThermoFisher, A-21127, 1:2000), goat-anti-mouse-IgG2a-Cross-Adsorbed-Alexa647 (ThermoFisher, A-21241, 1:1000), and goat-anti-rabbit-IgG (H+L)-Highly-Cross-Adsorbed-Alexa488 (Invitrogen, A11034, 1:800) diluted in blocking buffer were added and the plates were incubated for 90 min at room temperature. Next, cells were incubated with 572 nM = 200 ng/ml of DAPI (4', 6-diamidino-2-phenylindole) in PBS for 10 min, and washed 3 x 5 min with PBS.

Antibodies

The antibodies used in this study were generated within the HPA project except for the marker antibodies for cilia (targeting ARL13B, Abcam, ab136648, RRID:AB_3073658) and basal bodies (targeting PCNT, Abcam, ab28144, RRID:AB_2160664) and antibodies for STAT5 (HPA internal ID: CAB005418, Santa Cruz Biotechnology, sc-836, RRID:AB_632445), AXIN1 (HPA internal ID: CAB012987, Thermo Fisher Scientific, 34-5900, RRID:AB_2533178), SSTR3 (HPA internal ID: CAB022647, Merck Millipore, AB9774, RRID:AB_673004), WASHC5 (HPA internal ID: CAB034219, Santa Cruz Biotechnology, sc-87444, RRID:AB_2130519), and NRAS (HPA internal ID: CAB079912,, Thermo Fisher Scientific, 703435, RRID:AB_2784586). Supplementary Table 11 lists the HPA antibodies applied for revealing the 654 ciliary proteins.

All HPA antibodies are rabbit polyclonal antibodies generated using recombinant protein epitope signature tags (PrEST) as antigens for immunization [118]. The PrESTs are designed to enable the antibody to bind specifically to as many isoforms of the target protein as possible. The resulting antibodies were affinity purified using the PrEST antigen as an affinity ligand. Commercial antibodies were provided by the suppliers and used according to the supplier's recommendations. As previously described, the antibodies were initially quality controlled for sensitivity and lack of cross-reactivity to other proteins using western blotting and protein arrays [118]. Antibodies that passed the initial quality assessment, with no literature contradicting the results obtained in immunofluorescence (IF), were labeled 'approved'. If there was independent data in UniProt supporting the results in IF, the antibody was labeled 'supported'. For enhanced application-specific validation, we used the strategies outlined by the International Working Group for Antibody Validation (IWGAV) [119], including i) validation by gene silencing/knockout, ii) validation by co-staining of fluorescent protein-tagged protein expressed at endogenous levels, iii) validation by independent antibody targeting a different epitope, and iv) capture validation by mass

spectrometry [119,120]. If the antibody had been validated according to the IWGAV guidelines, it was labeled ‘enhanced’.

Fluorescence image acquisition of cells

All fluorescent images of cells were acquired with an inverted Leica SP8 confocal microscope equipped with a motorized and piezo z stage, an HC PL APO CS2 63×/1.20 water-immersion objective (Leica Microsystems, Mannheim, Germany), Laser Diodes 405, 488, 552, and 638, and HyD detectors. The settings for each image were Pinhole 1 Airy unit, 16-bit acquisition, 1.28x zoom, 2048x2048 pixels field of view, 700 Hz scan speed, resulting in a pixel size of 0.07 µm. All channels were detected on HyD detectors in multiple individual series to reduce bleed through: (1) DAPI and Cilia (Alexa 647) were detected, (2) the protein of interest was detected (Alexa 488), (3) the basal body channel was detected (Alexa 555). The detector gain and the laser intensity for the protein of interest (Alexa 488) channel were constant for all images acquired. On every plate a negative control (no primary rabbit antibody) was included and recorded to confirm that no nonspecific signals were visible in the Alexa488 channel. Detector gains and laser intensities for the other channels were minimally adjusted between different plates and cell lines, if needed (the different cell lines showed different strength of ARL13B PCNT and DAPI signals and thus, customization was required). Acquisition of images was conducted fully automatically, at least 4 images at random positions per well were acquired. If these images did not contain cilia or were deemed insufficient for deciding on a subcellular location (in the IF image annotation workflow described below), additional images at random positions were acquired. For ASC52telo cells, in this additional acquisition step, the field of views were placed manually in ciliated regions with many cells (without looking at the protein of interest channel).

Image processing

Images were exported to OME-TIFF format through Leica LASX’s inbuilt 3D viewer software. The OME-TIFF images were next reprocessed by a custom-written ImageJ plugin that complements and corrects metadata in the OME-XML strings in the tiff files based on the xml-based metadata files co-saved from Leica´s LAS-X software. Next all images were imported into the Laboratory Internal Management System (LIMS) of the Human Protein Atlas. Here, the intensity range for all channels was adjusted by an automatic script lowering the maximum displayed intensity value to improve visibility of stainings. The maximum display intensity was, however, never allowed to fall below 10,000 a.u., which corresponds to a value where in a negative control staining no signals were visible (Negative control staining was obtained by keeping all markers and secondary antibodies in the procedure but leaving out an antibody for the protein of interest). During manual annotation (see below), the maximum displayed intensity value was - if needed - further adjusted to better visualize ciliary signals but also never allowed to be set below 10,000 a.u. For display on the https://www.proteinatlas.org webpage, all images were converted from TIFF to JPEG file format based on the set maximum display intensity range.

Image annotation

The subcellular location of each protein was manually determined based on the signal pattern and relation to the markers for nucleus (DAPI), cilia (ARL13B), and basal bodies (PCNT). 35

different subcellular locations (Intermediate filaments, Actin cytoskeleton, Microtubules, Microtubule ends, Centriolar satellites, Mitochondria, Aggresome, Cytosol, Cytoplasmic bodies, Rods & Rings, ER, Golgi, Vesicles, Peroxisomes, Endosomes, Lysosomes, Lipid droplets, Plasma membrane, Cell Junctions, Focal Adhesions, Nucleoplasm, Nuclear membrane, Nucleoli, Nucleoli Fibrillar center, Nucleoli rim, Nuclear speckles, Nuclear bodies, Micronucleus, Kinetochore, Mitotic chromosome, Cytokinetic bridge, Midbody, Midbody ring, Cleavage furrow, Mitotic spindle), the standard for the subcellular section of the human protein atlas[26], and four additional cilia-related locations were annotated for all images: primary cilium, basal body, primary cilium tip, primary cilium transition zone. If more than one location was detected, they were defined as the main or additional location depending on the relative signal strength between the location and the most common location when including multiple cell lines, including also non-ciliated cell lines in the HPA. Variation between single cells was annotated as variation in the intensity or spatial distribution based on a visual inspection. The staining was not annotated if considered negative or unspecific.

Of note, it is likely that in many cases - given the resolution of the method - it was not possible to distinguish a transition zone and primary cilium staining from an only primary cilium staining unless the transition zone staining is significantly brighter than the whole cilium staining. The proteins annotated to stain the transition zone showed a clear only transition zone staining in at least one cell line. The same applied to ciliary tip proteins.

While the HPA antibodies are highly validated, we cannot exclude that some of the revealed proteins may be false positives due to unspecific binding or cross-reactivity of the antibody; the likelihood for this is particularly low in light of the significant diversity we observe in the ciliary proteins. Given the limitations with antibodies and the difficulty studying a tiny structure like primary cilia, we do not conclude that the proteins not detected in cilia in any cell lines are in fact not in cilia. Biological reasons for not detecting them may be that they localize to cilia only in other cell types or under other culturing conditions, such as upon stimulation with a receptor ligands, or that they are of extremely low abundance.

Image analysis

OME-TIFF files for individual channels and slices were fetched from the internal image database of the Human Protein Atlas and composed into z-stack tif-files. To segment individual cilia and basal body from the 3-dimensional image stack, we firstly blurred the image using a Gaussian kernel (standard deviation of 1) and subtracted the background which is obtained by blurring the original image using a larger Gaussian kernel (standard deviation of 10). Next, we set threshold values to segment the cilia and basal body objects. We empirically found that Otsu thresholding and 10 times of triangle thresholding values work best for basal body and cilia, respectively. To refine the segmented structures, we performed image opening using a ball kernel of radius 1, then removed small unconnected objects from the segmentation (objects smaller than 75 and 200 pixels for basal body and cilia, respectively). We also removed the falsely segmented cilia that is not attached to any segmented basal bodies.

To analyze how many cells and cilia were in the data set, as well as the ciliation rate, we used a new version of CiliaQ that tracks basal bodies / centrosomes and cilia (CiliaQ Version v0.2.1) [84].

Considering the different sizes of intensity profiles associated with each cilia, we projected each path onto the same 1-dimensional grid from 0 to 1 with 100 intervals (the starting and ending points are mapped to 0 and 1 respectively) and interpolated the profile according to the grid. Specifically, for cilia that are longer than 1.16 micrometers, we partitioned it into two pieces (0 to 1.16 micrometers and 1.16 micrometers to its end) and projected the first part onto the grid of 0 - 20 and the second part onto the grid of 21 - 100. For the cilia shorter than 1.16 micrometers, we projected it onto the grid points 0 to 20 and filled the vector by 0s after that. The rationale here is to prevent stretching protein intensity at the bottom of short cilia too much and to better characterize the non-deformed basal body / transition zone. The stretching creates ciliary intensity profiles representing vectors of a fixed length of 100. All profiles were further normalized by the maximal values among all profiles belonging to the same staining and smoothened each profile using a 1-dimensional Gaussian kernel (standard deviation of 8). To visualize the differences between profiles associated with proteins at different subcellular structures, for example, proteins located at basal body, primary cilium, primary cilium tip and transition zone, we plotted the median, 25 and 75 percentiles among intensity profiles at each grid point along the normalized cilia path for proteins localized in each of those structures.

Hierarchical clustering of intensity profiles

Single-cilia intensity profiles were aggregated to mean ciliary intensity profiles per protein and cell line utilizing Python v3.10. Each average profile was scaled by dividing all intensity values by the maximum intensity value of that profile. Hierarchical clustering of the aggregated profiles was conducted for each cell line, employing the pdist() and linkage() functions from the SciPy library (v1.14.0) [121] with Euclidean distance and the Unweighted Pair Group Method with Arithmetic Mean (UPGMA). Clusters were identified using the AgglomerativeClustering() function from scikit-learn v1.5.1 [122], with a distance threshold chosen to reflect the similarity matrix of the clustered profiles. Finally, the clustered average intensity profiles were visualized using the clustermap() and heatmap() functions from the seaborn library v0.13.2. Additionally, a functional enrichment analysis for each cluster was performed using the G:Profiler Python library v1.0.0 [123]. GO Biological Processes and GO Molecular Functions ontologies were used, the human genome was set as background, g:SCS algorithm was used to compute multiple testing corrections for p-values and a significance threshold of $p<0.05$ was selected. The resulting significant terms were simplified by removing all terms that were significant for more than one cluster per cell line.

Multilocalization analysis

To assess whether ciliary proteins localize to significantly more subcellular compartments than the overall proteome, we first counted the number of subcellular compartments annotated for each protein in the Human Protein Atlas. We then compared the distribution of the number of subcellular localization annotations for all proteins in the HPA (with any subcellular location annotation) to that of ciliary proteins—specifically, those annotated with "primary cilium tip,"

"primary cilium," and "primary cilium transition zone." A two-sided Mann-Whitney U test was used to determine statistical significance, with a P-value threshold set at $P < 0.01$.

To study the locations, where multilocalizing proteins were observed, the annotations on the staining level (data split by protein and cell line) from all cell lines were converted into edges with the python package networkx (version 3.2) and next plotted using the python package d3blocks (version 1.4.6).

Functional enrichment analyses

Functional enrichment analyses were conducted in R v4.4.1 using clusterProfiler v4.12.6 [124], enrichplot v1.24.4, and simplifyEnrichment v1.14.1 [125]. Overrepresentation of Gene Ontology Biological Process terms compared to all human genes was computed using the compareCluster function of clusterProfiler with org.Hs.eg.db as annotation database. The results were controlled for multiple hypothesis testing by calculating adjusted P values using the Benjamini-Hochberg Procedure and q values and restricting the results to adjusted P values < 0.01 and q values < 0.01. Results were visualized using the dotplot function from enrichplot. Additionally, the resulting list of significantly enriched GO terms for each variable in each comparison was simplified by calculating and clustering the corresponding semantic similarity matrix of the significant GO terms. Relational similarity was used as the similarity measure and binary_cut as clustering method. For each of the resulting clusters, a word cloud was drawn summarizing the biological functions with keywords in every GO term cluster. For this, the enrichment of keywords compared to the background GO vocabulary is determined using Fisher's Exact test and mapped to the fontsize of the keywords in the word clouds. Overrepresentation of Reactome pathways was determined equivalently, but were not further simplified.
To compare ciliary locations to cellular locations the 35 HPA locations were simplified into four groups: cytoplasm, membrane, nucleus and mitotic. Cytoplasm collected annotations for Intermediate filaments, Actin cytoskeleton, Microtubules, Microtubule ends, Centriolar satellites, Mitochondria, Aggresome, Cytosol, Cytoplasmic bodies, Rods & Rings. Membrane contained the endo-membrane system, collecting annotations for ER, Golgi, Vesicles, Peroxisomes, Endosomes, Lysosomes, Lipid droplets, Plasma membrane, Cell Junctions, Focal Adhesions. Nucleus collected annotations for Nucleoplasm, Nuclear membrane, Nucleoli, Nucleoli Fibrillar center, Nucleoli rim, Nuclear speckles, Nuclear bodies, Micronucleus. Mitotic collected annotations for Kinetochore, Mitotic chromosome, Cytokinetic bridge, Midbody, Midbody ring, Cleavage furrow, Mitotic spindle.

Human tissue sample preparation

The tissue sample preparation protocol used was the same as that described earlier by Danielsson et al. [126]. The tissue samples were processed following Swedish laws and regulation, obtained from the Department of Pathology, Uppsala University Hospital, Sweden, as included in the sample collection governed by the Uppsala Biobank (http://www.uppsalabiobank.uu.se/en/). All human tissue samples used were anonymized in accordance with an approval and advisory report from the Uppsala Ethical Review Board (Dnr Ups 02-577). Tissue MicroArrays (TMA) were constructed with strategies used in the Human Protein Atlas previously described [127,128], in

Formalin-fixed paraffin-embedded (FFPE) format. In summary, hematoxylin-eosin stained tissue sections from FFPE donor blocks were examined to confirm histology and identify representative regions for sampling into the TMA. Normal tissue was characterized as microscopically normal, predominantly sourced from proximity areas to surgically excised tumors. TMA blocks were created, each containing triplicate 1 mm cores from the different types of normal tissue.

Immunofluorescence staining of tissues

We used the same indirect immunofluorescence staining protocol described by Martinez Casals et al. [129]. with some adjustments. In brief: single section from each of the human TMA FFPE blocks was sectioned at 4 µm thickness. Each section was dewaxed and underwent heat-induced epitope retrieval (HIER) treatment using pH 9 EDTA buffer (Akoya Biosciences, AR900250ML) in a pressure cooker (Bio SB TintoRetriever, BSB-7087) at 114–121 °C during 20 minutes. After two ddH2O washes, the material was exposed to a photobleaching procedure to reduce tissue autofluorescence; following a blocking step using TNB buffer containing 0.1 M Tris-HCl /0.15 M NaCl/0.5% blocking reagent pH 7.5 (Akoya, SKU FP1020) for 30 min. Primary antibodies targeting ARL13B (Abcam, ab136648, RRID:AB_3073658, mouse IgG2a, 1:300), PCNT (Abcam, ab28144, RRID:AB_2160664, mouse IgG1, 1:500), and CFAP300 (HPA, HPA038585, rabbit polyclonal, 1:100) were diluted in antibody diluent containing 0.3 % Triton (Sigma Aldrich, T8787) 1x PBS pH 7.4 and added on the TMA section to be incubated overnight at 4°C. The next day, the material was washed with TBS-T and blocked using TNB for 30 min. Secondary antibodies, goat-anti-mouse-IgG2a-Cross-Adsorbed-Alexa647 (ThermoFisher, A-21241, 1:600), goat-anti-mouse-IgG1-Cross-Adsorbed-Alexa555 (ThermoFisher, A-21127, 1:600), goat-anti-rabbit-IgG (H+L)-Highly-Cross-Adsorbed-Alexa488 (Invitrogen, A11034, 1:600) were diluted in TNB, containing Hoescht (ThermoFisher, H3570), and added on the section for 90 min incubation at room temperature. Lastly, the stained material was mounted with Fluoromount-G (Thermo Fisher Scientific, 00-4958-02) to proceed with image acquisition.

Fluorescence image acquisition of tissue cores from TMA sections

Regions of interest in the TMA were image acquired using Leica STELLARIS 8 confocal microscope equipped with a 63 HC PL APO 63x/1.20 water-immersion CS2 objective (Leica Microsystems. Mannheim, Germany). The settings for each image were Pinhole 1 Airy unit, 16-bit acquisition, 1x zoom, 2048x2048 pixels field of view, Z-stack size 9.1 µm, number of steps 14, resulting in a pixel size of 0.09 µm and a z-step size of 0.7 µm. Detectors used: HyD S1 was used for Hoechst channel, HyD H2 for A488 channel, Hyd S3 regarding the A555 channel, and Hyd X4 for Alexa 647 channel. The “Lightning” deconvolution software (Leica Microsystems, Mannheim, Germany), which was integrated into the microscope software, was used to deconvolve the images after recording.

Immunohistochemistry images

The immunohistochemical stainings were performed as part of the regular Human Protein Atlas workflow, as described elsewhere. [25,32]

Exploration of clinical databases

Clinical samples analyzed at the Karolinska University Hospital by whole genome sequencing (WGS) were searched for interesting variants in genes who were classified in OMIM [96] as without a phenotype or not annotated in OMIM at all (Fig. 6A, Supplementary Table 10). The overall detailed analytical process of WGS has previously been described in Stranneheim et al. [112] and in Ek et al. [113] Clinical WGS data from three groups of patients were queried: 1) patients with a suspected ciliopathy disorder without a causative variant found in a clinical WGS (n=157), 2) fetuses with an ultrasound-detected malformation without a causative variant found in a clinical WGS (n=470) and 3) patients who had undergone a clinical patient-parental trio WGS analysis (n>1,500). We searched for potentially clinically relevant single nucleotide variants in the WGS data from these three patient groups by one gene at a time, filtering for the found variants so that only frameshift variants, nonsense variants and predicted splicing variants in a homozygous, compound heterozygous or *de novo* state were retained.

Data availability

The data presented in this study, including staining annotation, is available in the Human Protein Atlas (v24) at https://www.proteinatlas.org.

Acknowledgement

This research was funded by grants from Göran Gustafsson Foundation, Erling Persson Foundation, Chan-Zuckerberg Biohub, and Knut and Alice Wallenberg Foundation to EL (KAW 2021.0346) as well as to MU (HPA). JNH was supported by a Postdoctoral Fellowship from the Wenner-Gren Foundations, and by an EMBO Postdoctoral Fellowship (ALTF 556-2022).

Author contribution

JNH, UA, and EL conceived the project and designed the study. JNH, UA, AJ, KT, AMC, EP, JF, and AB conducted experiments. UA, JNH, KT, JF, EL, and DM annotated images. JNH, UA, EL, HS, KK, EW, CW, and DM analyzed and interpreted data. MU and CLB contributed to the discussion and critical reagents. JNH, UA, and EL wrote the paper. ADV and AL supervised the clinical analysis. EL supervised the project. KVF, FJ, and UA built the cilia atlas in HPA. All authors edited and commented on the manuscript.

References

1. Mill, P., Christensen, S.T., and Pedersen, L.B. (2023). Primary cilia as dynamic and diverse signalling hubs in development and disease. Nat Rev Genet. https://doi.org/10.1038/s41576-023-00587-9.
2. Reiter, J.F., and Leroux, M.R. (2017). Genes and molecular pathways underpinning ciliopathies. Nature reviews. Molecular cell biology *18*, 533–547. https://doi.org/10.1038/nrm.2017.60.
3. Pazour, G.J., and Witman, G.B. (2003). The vertebrate primary cilium is a sensory

organelle. Current opinion in cell biology *15*, 105–110.
4. Gopalakrishnan, J., Feistel, K., Friedrich, B.M., Grapin-Botton, A., Jurisch-Yaksi, N., Mass, E., Mick, D.U., Müller, R., May-Simera, H., Schermer, B., et al. (2023). Emerging principles of primary cilia dynamics in controlling tissue organization and function. The EMBO Journal *42*, e113891. https://doi.org/10.15252/embj.2023113891.
5. Breslow, D.K., and Holland, A.J. (2019). Mechanism and Regulation of Centriole and Cilium Biogenesis. Annu. Rev. Biochem. *88*, 691–724. https://doi.org/10.1146/annurev-biochem-013118-111153.
6. Anderson, R.G. (1972). The three-dimensional structure of the basal body from the rhesus monkey oviduct. J. Cell Biol. *54*, 246–265. https://doi.org/10.1083/jcb.54.2.246.
7. Gibbons, I.R., and Grimstone, A.V. (1960). On flagellar structure in certain flagellates. J. Biophys. Biochem. Cytol. *7*, 697–716. https://doi.org/10.1083/jcb.7.4.697.
8. O'Toole, E.T., Giddings, T.H., and Dutcher, S.K. (2007). Understanding microtubule organizing centers by comparing mutant and wild-type structures with electron tomography. Methods Cell Biol. *79*, 125–143. https://doi.org/10.1016/S0091-679X(06)79005-7.
9. Ringo, D.L. (1967). Flagellar motion and fine structure of the flagellar apparatus in Chlamydomonas. J. Cell Biol. *33*, 543–571. https://doi.org/10.1083/jcb.33.3.543.
10. Moran, A.L., Louzao-Martinez, L., Norris, D.P., Peters, D.J.M., and Blacque, O.E. (2023). Transport and barrier mechanisms that regulate ciliary compartmentalization and ciliopathies. Nat Rev Nephrol. https://doi.org/10.1038/s41581-023-00773-2.
11. Hu, Q., Milenkovic, L., Jin, H., Scott, M.P., Nachury, M.V., Spiliotis, E.T., and Nelson, W.J. (2010). A septin diffusion barrier at the base of the primary cilium maintains ciliary membrane protein distribution. Science *329*, 436–439. https://doi.org/10.1126/science.1191054.
12. Gilula, N.B., and Satir, P. (1972). The ciliary necklace. A ciliary membrane specialization. The Journal of cell biology *53*, 494–509. https://doi.org/10.1083/jcb.53.2.494.
13. Yang, T.T., Chong, W.M., Wang, W.J., Mazo, G., Tanos, B., Chen, Z., Tran, T.M.N., Chen, Y.D., Weng, R.R., Huang, C.E., et al. (2018). Super-resolution architecture of mammalian centriole distal appendages reveals distinct blade and matrix functional components. Nature communication *9*, 2023. https://doi.org/10.1038/s41467-018-04469-1.
14. Garcia, G., Raleigh, D.R., and Reiter, J.F. (2018). How the Ciliary Membrane Is Organized Inside-Out to Communicate Outside-In. Curr. Biol. *28*, R421–R434. https://doi.org/10.1016/j.cub.2018.03.010.
15. Pazour, G.J., Agrin, N., Leszyk, J., and Witman, G.B. (2005). Proteomic analysis of a eukaryotic cilium. J. Cell Biol. *170*, 103–113. https://doi.org/10.1083/jcb.200504008.
16. Gigante, E.D., and Caspary, T. (2020). Signaling in the primary cilium through the lens of the Hedgehog pathway. WIREs Dev. Biol. *9*, e377. https://doi.org/10.1002/wdev.377.
17. Shinde, S.R., Nager, A.R., and Nachury, M.V. (2020). Ubiquitin chains earmark GPCRs for BBSome-mediated removal from cilia. J. Cell Biol. *219*. https://doi.org/10.1083/jcb.202003020.
18. Ye, F., Nager, A.R., and Nachury, M.V. (2018). BBSome trains remove activated GPCRs from cilia by enabling passage through the transition zone. J. Cell Biol. *217*, 1847–1868. https://doi.org/10.1083/jcb.201709041.
19. Spasic, M., and Jacobs, C.R. (2017). Lengthening primary cilia enhances cellular mechanosensitivity. Eur. Cell. Mater. *33*, 158–168. https://doi.org/10.22203/eCM.v033a12.
20. Mick, D.U., Rodrigues, R.B., Leib, R.D., Adams, C.M., Chien, A.S., Gygi, S.P., and Nachury, M.V. (2015). Proteomics of Primary Cilia by Proximity Labeling. Dev. Cell *35*, 497–512. https://doi.org/10.1016/j.devcel.2015.10.015.
21. Kohli, P., Hohne, M., Jungst, C., Bertsch, S., Ebert, L.K., Schauss, A.C., Benzing, T., Rinschen, M.M., and Schermer, B. (2017). The ciliary membrane-associated proteome reveals actin-binding proteins as key components of cilia. EMBO rep. *18*, 1521–1535.

https://doi.org/10.15252/embr.201643846.
22. May, E.A., Kalocsay, M., D'Auriac, I.G., Schuster, P.S., Gygi, S.P., Nachury, M.V., and Mick, D.U. (2021). Time-resolved proteomics profiling of the ciliary Hedgehog response. J. Cell Biol. *220*. https://doi.org/10.1083/jcb.202007207.
23. Gupta, G.D., Coyaud, E., Goncalves, J., Mojarad, B.A., Liu, Y., Wu, Q., Gheiratmand, L., Comartin, D., Tkach, J.M., Cheung, S.W., et al. (2015). A Dynamic Protein Interaction Landscape of the Human Centrosome-Cilium Interface. Cell *163*, 1484–1499. https://doi.org/10.1016/j.cell.2015.10.065.
24. Aslanyan, M.G., Doornbos, C., Diwan, G.D., Anvarian, Z., Beyer, T., Junger, K., Van Beersum, S.E.C., Russell, R.B., Ueffing, M., Ludwig, A., et al. (2023). A targeted multi-proteomics approach generates a blueprint of the ciliary ubiquitinome. Front. Cell Dev. Biol. *11*, 1113656. https://doi.org/10.3389/fcell.2023.1113656.
25. Uhlén, M., Fagerberg, L., Hallström, B.M., Lindskog, C., Oksvold, P., Mardinoglu, A., Sivertsson, Å., Kampf, C., Sjöstedt, E., Asplund, A., et al. (2015). Tissue-based map of the human proteome. Science *347*, 1260419. https://doi.org/10.1126/science.1260419.
26. Thul, P.J., Åkesson, L., Wiking, M., Mahdessian, D., Geladaki, A., Ait Blal, H., Alm, T., Asplund, A., Björk, L., Breckels, L.M., et al. (2017). A subcellular map of the human proteome. Science *356*, eaal3321. https://doi.org/10.1126/science.aal3321.
27. Rambhatla, L., Chiu, C.-P., Glickman, R.D., and Rowe-Rendleman, C. (2002). In vitro differentiation capacity of telomerase immortalized human RPE cells. Invest Ophthalmol Vis Sci *43*, 1622–1630.
28. Wieser, M., Stadler, G., Jennings, P., Streubel, B., Pfaller, W., Ambros, P., Riedl, C., Katinger, H., Grillari, J., and Grillari-Voglauer, R. (2008). hTERT alone immortalizes epithelial cells of renal proximal tubules without changing their functional characteristics. American Journal of Physiology-Renal Physiology *295*, F1365–F1375. https://doi.org/10.1152/ajprenal.90405.2008.
29. Wolbank, S., Stadler, G., Peterbauer, A., Gillich, A., Karbiener, M., Streubel, B., Wieser, M., Katinger, H., Van Griensven, M., Redl, H., et al. (2009). *Telomerase* Immortalized Human Amnion- and Adipose-Derived Mesenchymal Stem Cells: Maintenance of Differentiation and Immunomodulatory Characteristics. Tissue Engineering Part A *15*, 1843–1854. https://doi.org/10.1089/ten.tea.2008.0205.
30. Paridaen, J.T., Wilsch-Brauninger, M., and Huttner, W.B. (2013). Asymmetric inheritance of centrosome-associated primary cilium membrane directs ciliogenesis after cell division. Cell *155*, 333–344. https://doi.org/10.1016/j.cell.2013.08.060.
31. Vasquez, S.S.V., van Dam, J., and Wheway, G. (2021). An updated SYSCILIA gold standard (SCGSv2) of known ciliary genes, revealing the vast progress that has been made in the cilia research field. Mol. Biol. Cell *32*, br13. https://doi.org/10.1091/mbc.E21-05-0226.
32. Lindskog, C., Norradin, F.H., Digre, A., Méar, L., Schutten, R., Lundberg, E., Hansen, J., and Uhlén, M. (2024). A high-resolution spatial map of cilia-associated proteins based on characterization of the human fallopian tube-specific proteome. Preprint, https://doi.org/10.21203/rs.3.rs-3914234/v1 https://doi.org/10.21203/rs.3.rs-3914234/v1.
33. Ishikawa, H., Thompson, J., Yates, J.R., and Marshall, W.F. (2012). Proteomic analysis of mammalian primary cilia. Curr. Biol. *22*, 414–419. https://doi.org/10.1016/j.cub.2012.01.031.
34. Karunakaran, K.B., Chaparala, S., Lo, C.W., and Ganapathiraju, M.K. (2020). Cilia interactome with predicted protein-protein interactions reveals connections to Alzheimer's disease, aging and other neuropsychiatric processes. Sci. Rep. *10*, 15629. https://doi.org/10.1038/s41598-020-72024-4.
35. van Dam, T.J.P., Kennedy, J., van der Lee, R., de Vrieze, E., Wunderlich, K.A., Rix, S., Dougherty, G.W., Lambacher, N.J., Li, C., Jensen, V.L., et al. (2019). CiliaCarta: An

integrated and validated compendium of ciliary genes. PloS one *14*, e0216705. https://doi.org/10.1371/journal.pone.0216705.
36. Pir, M.S., Begar, E., Yenisert, F., Demirci, H.C., Korkmaz, M.E., Karaman, A., Tsiropoulou, S., Firat-Karalar, E.N., Blacque, O.E., Oner, S.S., et al. (2024). CilioGenics: an integrated method and database for predicting novel ciliary genes. Nucleic Acids Research, gkae554. https://doi.org/10.1093/nar/gkae554.
37. Elliott, K.H., Balchand, S.K., Bonatto Paese, C.L., Chang, C.-F., Yang, Y., Brown, K.M., Rasicci, D.T., He, H., Thorner, K., Chaturvedi, P., et al. (2023). Identification of a heterogeneous and dynamic ciliome during embryonic development and cell differentiation. Development *150*, dev201237. https://doi.org/10.1242/dev.201237.
38. Nevers, Y., Prasad, M.K., Poidevin, L., Chennen, K., Allot, A., Kress, A., Ripp, R., Thompson, J.D., Dollfus, H., Poch, O., et al. (2017). Insights into Ciliary Genes and Evolution from Multi-Level Phylogenetic Profiling. Mol. Biol. Evol. *34*, 2016–2034. https://doi.org/10.1093/molbev/msx146.
39. Sigg, M.A., Menchen, T., Lee, C., Johnson, J., Jungnickel, M.K., Choksi, S.P., Garcia, G., Busengdal, H., Dougherty, G.W., Pennekamp, P., et al. (2017). Evolutionary Proteomics Uncovers Ancient Associations of Cilia with Signaling Pathways. Dev. Cell *43*, 744-762 e11. https://doi.org/10.1016/j.devcel.2017.11.014.
40. Breslow, D.K., Hoogendoorn, S., Kopp, A.R., Morgens, D.W., Vu, B.K., Kennedy, M.C., Han, K., Li, A., Hess, G.T., Bassik, M.C., et al. (2018). A CRISPR-based screen for Hedgehog signaling provides insights into ciliary function and ciliopathies. Nat. Genet. https://doi.org/10.1038/s41588-018-0054-7.
41. Pusapati, G.V., Kong, J.H., Patel, B.B., Krishnan, A., Sagner, A., Kinnebrew, M., Briscoe, J., Aravind, L., and Rohatgi, R. (2018). CRISPR Screens Uncover Genes that Regulate Target Cell Sensitivity to the Morphogen Sonic Hedgehog. Dev. Cell *44*, 113-129 e8. https://doi.org/10.1016/j.devcel.2017.12.003.
42. Blackburn, K., Bustamante-Marin, X., Yin, W., Goshe, M.B., and Ostrowski, L.E. (2017). Quantitative Proteomic Analysis of Human Airway Cilia Identifies Previously Uncharacterized Proteins of High Abundance. J. Proteome Res. *16*, 1579–1592. https://doi.org/10.1021/acs.jproteome.6b00972.
43. Sim, H.J., Yun, S., Kim, H.E., Kwon, K.Y., Kim, G.-H., Yun, S., Kim, B.G., Myung, K., Park, T.J., and Kwon, T. (2020). Simple Method To Characterize the Ciliary Proteome of Multiciliated Cells. J. Proteome Res. *19*, 391–400. https://doi.org/10.1021/acs.jproteome.9b00589.
44. Baker, M.A., Naumovski, N., Hetherington, L., Weinberg, A., Velkov, T., and Aitken, R.J. (2013). Head and flagella subcompartmental proteomic analysis of human spermatozoa. Proteomics *13*, 61–74. https://doi.org/10.1002/pmic.201200350.
45. Amaral, A., Castillo, J., Estanyol, J.M., Ballescà, J.L., Ramalho-Santos, J., and Oliva, R. (2013). Human Sperm Tail Proteome Suggests New Endogenous Metabolic Pathways. Molecular & Cellular Proteomics *12*, 330–342. https://doi.org/10.1074/mcp.M112.020552.
46. Firat-Karalar, E.N., Sante, J., Elliott, S., and Stearns, T. (2014). Proteomic analysis of mammalian sperm cells identifies new components of the centrosome. Journal of Cell Science, jcs.157008. https://doi.org/10.1242/jcs.157008.
47. Tai, L., Yin, G., Huang, X., Sun, F., and Zhu, Y. (2023). In-cell structural insight into the stability of sperm microtubule doublet. Cell Discov *9*, 116. https://doi.org/10.1038/s41421-023-00606-3.
48. Zhou, L., Liu, H., Liu, S., Yang, X., Dong, Y., Pan, Y., Xiao, Z., Zheng, B., Sun, Y., Huang, P., et al. (2023). Structures of sperm flagellar doublet microtubules expand the genetic spectrum of male infertility. Cell *186*, 2897-2910.e19. https://doi.org/10.1016/j.cell.2023.05.009.
49. Gui, M., Croft, J.T., Zabeo, D., Acharya, V., Kollman, J.M., Burgoyne, T., Höög, J.L., and

Brown, A. (2022). SPACA9 is a lumenal protein of human ciliary singlet and doublet microtubules. Proc. Natl. Acad. Sci. U.S.A. *119*, e2207605119. https://doi.org/10.1073/pnas.2207605119.
50. Firat-Karalar, E.N., Rauniyar, N., Yates, J.R., and Stearns, T. (2014). Proximity interactions among centrosome components identify regulators of centriole duplication. Curr. Biol. *24*, 664–670. https://doi.org/10.1016/j.cub.2014.01.067.
51. Carden, S., Vitiello, E., Rosa E Silva, I., Holder, J., Quarantotti, V., Kishore, K., Roamio Franklin, V.N., D'Santos, C., Ochi, T., Van Breugel, M., et al. (2023). Proteomic profiling of centrosomes across multiple mammalian cell and tissue types by an affinity capture method. Developmental Cell *58*, 2393-2410.e9. https://doi.org/10.1016/j.devcel.2023.09.008.
52. Andersen, J.S., Wilkinson, C.J., Mayor, T., Mortensen, P., Nigg, E.A., and Mann, M. (2003). Proteomic characterization of the human centrosome by protein correlation profiling. Nature *426*, 570–574. https://doi.org/10.1038/nature02166.
53. Jakobsen, L., Vanselow, K., Skogs, M., Toyoda, Y., Lundberg, E., Poser, I., Falkenby, L.G., Bennetzen, M., Westendorf, J., Nigg, E.A., et al. (2011). Novel asymmetrically localizing components of human centrosomes identified by complementary proteomics methods: Centrosome proteomics. The EMBO Journal *30*, 1520–1535. https://doi.org/10.1038/emboj.2011.63.
54. Gheiratmand, L., Coyaud, E., Gupta, G.D., Laurent, E.M., Hasegan, M., Prosser, S.L., Gonçalves, J., Raught, B., and Pelletier, L. (2019). Spatial and proteomic profiling reveals centrosome-independent features of centriolar satellites. The EMBO Journal *38*, e101109. https://doi.org/10.15252/embj.2018101109.
55. Conkar, D., Culfa, E., Odabasi, E., Rauniyar, N., Yates, J.R., and Firat-Karalar, E.N. (2017). The centriolar satellite protein CCDC66 interacts with CEP290 and functions in cilium formation and trafficking. J. Cell Sci. *130*, 1450–1462. https://doi.org/10.1242/jcs.196832.
56. Bennett, H.W., Gustavsson, A.K., Bayas, C.A., Petrov, P.N., Mooney, N., Moerner, W.E., and Jackson, P.K. (2020). Novel fibrillar structure in the inversin compartment of primary cilia revealed by 3D single-molecule superresolution microscopy. Molecular biology of the cell *31*, 619–639. https://doi.org/10.1091/mbc.E19-09-0499.
57. Pusapati, G.V., Hughes, C.E., Dorn, K.V., Zhang, D., Sugianto, P., Aravind, L., and Rohatgi, R. (2014). EFCAB7 and IQCE Regulate Hedgehog Signaling by Tethering the EVC-EVC2 Complex to the Base of Primary Cilia. Developmental Cell *28*, 483–496. https://doi.org/10.1016/j.devcel.2014.01.021.
58. Boehlke, C., Bashkurov, M., Buescher, A., Krick, T., John, A.-K., Nitschke, R., Walz, G., and Kuehn, E.W. (2010). Differential role of Rab proteins in ciliary trafficking: Rab23 regulates smoothened levels. J Cell Sci *123*, 1460–1467. https://doi.org/10.1242/jcs.058883.
59. Chi, S., Xie, G., Liu, H., Chen, K., Zhang, X., Li, C., and Xie, J. (2012). Rab23 negatively regulates Gli1 transcriptional factor in a Su(Fu)-dependent manner. Cell Signal *24*, 1222–1228. https://doi.org/10.1016/j.cellsig.2012.02.004.
60. Cho, J.H., Li, Z.A., Zhu, L., Muegge, B.D., Roseman, H.F., Lee, E.Y., Utterback, T., Woodhams, L.G., Bayly, P.V., and Hughes, J.W. (2022). Islet primary cilia motility controls insulin secretion. Sci. Adv. *8*, eabq8486. https://doi.org/10.1126/sciadv.abq8486.
61. Eymael, J., Willemsen, B., Xu, J., Mooren, F., Steenbergen, E., Wetzels, J.F., Dijkman, H., Jansen, J., Van der Vlag, J., and Smeets, B. (2022). Motile Cilia on Kidney Proximal Tubular Epithelial Cells Are Associated With Tubular Injury and Interstitial Fibrosis. Front. Cell Dev. Biol. *10*, 765887. https://doi.org/10.3389/fcell.2022.765887.
62. van Rijssel, J., and van Buul, J.D. (2012). The many faces of the guanine-nucleotide exchange factor trio. Cell Adh Migr *6*, 482–487. https://doi.org/10.4161/cam.21418.

63. Sheu, S.-H., Upadhyayula, S., Dupuy, V., Pang, S., Deng, F., Wan, J., Walpita, D., Pasolli, H.A., Houser, J., Sanchez-Martinez, S., et al. (2022). A serotonergic axon-cilium synapse drives nuclear signaling to alter chromatin accessibility. Cell *185*, 3390-3407.e18. https://doi.org/10.1016/j.cell.2022.07.026.
64. Ota, M., Gonja, H., Koike, R., and Fukuchi, S. (2016). Multiple-Localization and Hub Proteins. PLoS ONE *11*, e0156455. https://doi.org/10.1371/journal.pone.0156455.
65. Mulvey, C.M., Breckels, L.M., Geladaki, A., Britovšek, N.K., Nightingale, D.J.H., Christoforou, A., Elzek, M., Deery, M.J., Gatto, L., and Lilley, K.S. (2017). Using hyperLOPIT to perform high-resolution mapping of the spatial proteome. Nat Protoc *12*, 1110–1135. https://doi.org/10.1038/nprot.2017.026.
66. Singh, N., and Bhalla, N. (2020). Moonlighting Proteins. Annu. Rev. Genet. *54*, 265–285. https://doi.org/10.1146/annurev-genet-030620-102906.
67. Mukhopadhyay, S., Wen, X., Chih, B., Nelson, C.D., Lane, W.S., Scales, S.J., and Jackson, P.K. (2010). TULP3 bridges the IFT-A complex and membrane phosphoinositides to promote trafficking of G protein-coupled receptors into primary cilia. Genes Dev. *24*, 2180–2193. https://doi.org/10.1101/gad.1966210.
68. Han, S., Miyoshi, K., Shikada, S., Amano, G., Wang, Y., Yoshimura, T., and Katayama, T. (2019). TULP3 is required for localization of membrane-associated proteins ARL13B and INPP5E to primary cilia. Biochemical and Biophysical Research Communications *509*, 227–234. https://doi.org/10.1016/j.bbrc.2018.12.109.
69. Fagan, R.R., Lee, D.F., Geron, M., Scherrer, G., Von Zastrow, M., and Ehrlich, A.T. (2024). Selective targeting of mu opioid receptors to primary cilia. Cell Reports *43*, 114164. https://doi.org/10.1016/j.celrep.2024.114164.
70. Santagata, S., Boggon, T.J., Baird, C.L., Gomez, C.A., Zhao, J., Shan, W.S., Myszka, D.G., and Shapiro, L. (2001). G-Protein Signaling Through Tubby Proteins. Science *292*, 2041–2050. https://doi.org/10.1126/science.1061233.
71. Hansen, J.N., Kaiser, F., Leyendecker, P., Stuven, B., Krause, J.H., Derakhshandeh, F., Irfan, J., Sroka, T.J., Preval, K.M., Desai, P.B., et al. (2022). A cAMP signalosome in primary cilia drives gene expression and kidney cyst formation. EMBO rep. *23*, e54315. https://doi.org/10.15252/embr.202154315.
72. Gnann, C., Cesnik, A., Sigaeva, A., Le, T., Sariyar, S., Mahdessian, D., Schutten, R., Raghavan, P., Leonetti, M.D., Lindskog, C., et al. (2024). Dissecting autonomous enzyme variability in single cells. Preprint, https://doi.org/10.1101/2024.10.03.616530 https://doi.org/10.1101/2024.10.03.616530.
73. Nguyen, T.D., Truong, M.E., and Reiter, J.F. (2022). The Intimate Connection Between Lipids and Hedgehog Signaling. Front. Cell Dev. Biol. *10*, 876815. https://doi.org/10.3389/fcell.2022.876815.
74. Kinnebrew, M., Iverson, E.J., Patel, B.B., Pusapati, G.V., Kong, J.H., Johnson, K.A., Luchetti, G., Eckert, K.M., McDonald, J.G., Covey, D.F., et al. (2019). Cholesterol accessibility at the ciliary membrane controls hedgehog signaling. eLife *8*, e50051. https://doi.org/10.7554/eLife.50051.
75. Wang, Y., Zhang, Y., Guo, X., Zheng, Y., Zhang, X., Feng, S., and Wu, H.-Y. (2023). CCP5 and CCP6 retain CP110 and negatively regulate ciliogenesis. BMC Biol *21*, 124. https://doi.org/10.1186/s12915-023-01622-1.
76. Adada, M.M., Orr-Gandy, K.A., Snider, A.J., Canals, D., Hannun, Y.A., Obeid, L.M., and Clarke, C.J. (2013). Sphingosine kinase 1 regulates tumor necrosis factor-mediated RANTES induction through p38 mitogen-activated protein kinase but independently of nuclear factor κB activation. J Biol Chem *288*, 27667–27679. https://doi.org/10.1074/jbc.M113.489443.
77. Maceyka, M., Sankala, H., Hait, N.C., Le Stunff, H., Liu, H., Toman, R., Collier, C., Zhang, M., Satin, L.S., Merrill, A.H., et al. (2005). SphK1 and SphK2, sphingosine kinase

isoenzymes with opposing functions in sphingolipid metabolism. J Biol Chem *280*, 37118–37129. https://doi.org/10.1074/jbc.M502207200.
78. Alvarez, S.E., Harikumar, K.B., Hait, N.C., Allegood, J., Strub, G.M., Kim, E.Y., Maceyka, M., Jiang, H., Luo, C., Kordula, T., et al. (2010). Sphingosine-1-phosphate is a missing cofactor for the E3 ubiquitin ligase TRAF2. Nature *465*, 1084–1088. https://doi.org/10.1038/nature09128.
79. Helenius, A., and Ritter, C. (2000). Recognition of local glycoprotein misfolding by the ER folding sensor UDP-glucose:glycoprotein glucosyltransferase. Nat. Struct Biol. *7*, 278–280. https://doi.org/10.1038/74035.
80. Wang, N., Seko, A., Takeda, Y., and Ito, Y. (2020). Glycan dependent refolding activity of ER glucosyltransferase (UGGT). Biochimica et Biophysica Acta (BBA) - General Subjects *1864*, 129709. https://doi.org/10.1016/j.bbagen.2020.129709.
81. Hua, K., and Ferland, R.J. (2017). Fixation methods can differentially affect ciliary protein immunolabeling. Cilia *6*, 5. https://doi.org/10.1186/s13630-017-0045-9.
82. Kinnebrew, M., Luchetti, G., Sircar, R., Frigui, S., Viti, L.V., Naito, T., Beckert, F., Saheki, Y., Siebold, C., Radhakrishnan, A., et al. (2021). Patched 1 reduces the accessibility of cholesterol in the outer leaflet of membranes. eLife *10*, e70504. https://doi.org/10.7554/eLife.70504.
83. Palander, O., El-Zeiry, M., and Trimble, W.S. (2017). Uncovering the Roles of Septins in Cilia. Front. Cell Dev. Biol. *5*. https://doi.org/10.3389/fcell.2017.00036.
84. Hansen, J.N., Rassmann, S., Stuven, B., Jurisch-Yaksi, N., and Wachten, D. (2021). CiliaQ: a simple, open-source software for automated quantification of ciliary morphology and fluorescence in 2D, 3D, and 4D images. Eur. Phys. J. E Soft Matter *44*, 18. https://doi.org/10.1140/epje/s10189-021-00031-y.
85. Bishop, G.A., Berbari, N.F., Lewis, J., and Mykytyn, K. (2007). Type III adenylyl cyclase localizes to primary cilia throughout the adult mouse brain. J. Comp. Neurol. *505*, 562–571. https://doi.org/10.1002/cne.21510.
86. Gigante, E.D., Taylor, M.R., Ivanova, A.A., Kahn, R.A., and Caspary, T. (2020). ARL13B regulates Sonic hedgehog signaling from outside primary cilia. eLife *9*, e50434. https://doi.org/10.7554/eLife.50434.
87. Ferent, J., Constable, S., Gigante, E.D., Yam, P.T., Mariani, L.E., Legué, E., Liem, K.F., Caspary, T., and Charron, F. (2019). The Ciliary Protein Arl13b Functions Outside of the Primary Cilium in Shh-Mediated Axon Guidance. Cell Reports *29*, 3356-3366.e3. https://doi.org/10.1016/j.celrep.2019.11.015.
88. Janke, C., and Montagnac, G. (2017). Causes and Consequences of Microtubule Acetylation. Curr. Biol. *27*, R1287–R1292. https://doi.org/10.1016/j.cub.2017.10.044.
89. Zlotina, A., Barashkova, S., Zhuk, S., Skitchenko, R., Usoltsev, D., Sokolnikova, P., Artomov, M., Alekseenko, S., Simanova, T., Goloborodko, M., et al. (2024). Characterization of pathogenic genetic variants in Russian patients with primary ciliary dyskinesia using gene panel sequencing and transcript analysis. Orphanet J Rare Dis *19*, 310. https://doi.org/10.1186/s13023-024-03318-3.
90. Jat, K.R., Faruq, M., Jindal, S., Bari, S., Soni, A., Sharma, P., Mathews, S., Shamim, U., Ahuja, V., Uppilli, B., et al. (2024). Genetics of 67 patients of suspected primary ciliary dyskinesia from India. Clinical Genetics, cge.14590. https://doi.org/10.1111/cge.14590.
91. Schultz, R., Elenius, V., Fassad, M.R., Freke, G., Rogers, A., Shoemark, A., Koistinen, T., Mohamed, M.A., Lim, J.S.Y., Mitchison, H.M., et al. (2022). CFAP300 mutation causing primary ciliary dyskinesia in Finland. Front. Genet. *13*, 985227. https://doi.org/10.3389/fgene.2022.985227.
92. Yiallouros, P.K., Kouis, P., Kyriacou, K., Evriviadou, A., Anagnostopoulou, P., Matthaiou, A., Tsiolakis, I., Pirpa, P., Michailidou, K., Potamiti, L., et al. (2021). Implementation of multigene panel NGS diagnosis in the national primary ciliary dyskinesia cohort of Cyprus:

An island with a high disease prevalence. Human Mutation *42*. https://doi.org/10.1002/humu.24196.
93. Aprea, I., Raidt, J., Höben, I.M., Loges, N.T., Nöthe-Menchen, T., Pennekamp, P., Olbrich, H., Kaiser, T., Biebach, L., Tüttelmann, F., et al. (2021). Defects in the cytoplasmic assembly of axonemal dynein arms cause morphological abnormalities and dysmotility in sperm cells leading to male infertility. PLoS Genet *17*, e1009306. https://doi.org/10.1371/journal.pgen.1009306.
94. Zietkiewicz, E., Bukowy-Bieryllo, Z., Rabiasz, A., Daca-Roszak, P., Wojda, A., Voelkel, K., Rutkiewicz, E., Pogorzelski, A., Rasteiro, M., and Witt, M. (2019). *CFAP300* : Mutations in Slavic Patients with Primary Ciliary Dyskinesia and a Role in Ciliary Dynein Arms Trafficking. Am J Respir Cell Mol Biol *61*, 440–449. https://doi.org/10.1165/rcmb.2018-0260OC.
95. Fassad, M.R., Shoemark, A., Le Borgne, P., Koll, F., Patel, M., Dixon, M., Hayward, J., Richardson, C., Frost, E., Jenkins, L., et al. (2018). C11orf70 Mutations Disrupting the Intraflagellar Transport-Dependent Assembly of Multiple Axonemal Dyneins Cause Primary Ciliary Dyskinesia. The American Journal of Human Genetics *102*, 956–972. https://doi.org/10.1016/j.ajhg.2018.03.024.
96. McKusick-Nathans Institute of Genetic Medicine, Johns Hopkins University (Baltimore, MD) Online Mendelian Inheritance in Man, OMIM®. https://omim.org/.
97. Sakurai, T. (2012). The role of NrCAM in neural development and disorders--beyond a simple glue in the brain. Mol Cell Neurosci *49*, 351–363. https://doi.org/10.1016/j.mcn.2011.12.002.
98. Yokoyama, K., Tezuka, T., Kotani, M., Nakazawa, T., Hoshina, N., Shimoda, Y., Kakuta, S., Sudo, K., Watanabe, K., Iwakura, Y., et al. (2011). NYAP: a phosphoprotein family that links PI3K to WAVE1 signalling in neurons: NYAPs link PI3K to WAVE1 in neurons. The EMBO Journal *30*, 4739–4754. https://doi.org/10.1038/emboj.2011.348.
99. Davare, M.A., Fortin, D.A., Saneyoshi, T., Nygaard, S., Kaech, S., Banker, G., Soderling, T.R., and Wayman, G.A. (2009). Transient Receptor Potential Canonical 5 Channels Activate Ca^{2+} /Calmodulin Kinase Iγ to Promote Axon Formation in Hippocampal Neurons. J. Neurosci. *29*, 9794–9808. https://doi.org/10.1523/JNEUROSCI.1544-09.2009.
100. Lucchesi, W., Mizuno, K., and Giese, K.P. (2011). Novel insights into CaMKII function and regulation during memory formation. Brain Research Bulletin *85*, 2–8. https://doi.org/10.1016/j.brainresbull.2010.10.009.
101. Araki, T., and Wakatsuki, S. (2019). Regulation of neuronal/axonal degeneration by ZNRF1 ubiquitin ligase. Neuroscience Research *139*, 21–25. https://doi.org/10.1016/j.neures.2018.07.008.
102. Yoshida, K., Watanabe, M., and Hatakeyama, S. (2009). ZNRF1 interacts with tubulin and regulates cell morphogenesis. Biochemical and Biophysical Research Communications *389*, 506–511. https://doi.org/10.1016/j.bbrc.2009.09.011.
103. Hu, H.-B., Song, Z.-Q., Song, G.-P., Li, S., Tu, H.-Q., Wu, M., Zhang, Y.-C., Yuan, J.-F., Li, T.-T., Li, P.-Y., et al. (2021). LPA signaling acts as a cell-extrinsic mechanism to initiate cilia disassembly and promote neurogenesis. Nat Commun *12*, 662. https://doi.org/10.1038/s41467-021-20986-y.
104. Loskutov, Y.V., Griffin, C.L., Marinak, K.M., Bobko, A., Margaryan, N.V., Geldenhuys, W.J., Sarkaria, J.N., and Pugacheva, E.N. (2018). LPA signaling is regulated through the primary cilium: a novel target in glioblastoma. Oncogene *37*, 1457–1471. https://doi.org/10.1038/s41388-017-0049-3.
105. Walia, V., Cuenca, A., Vetter, M., Insinna, C., Perera, S., Lu, Q., Ritt, D.A., Semler, E., Specht, S., Stauffer, J., et al. (2019). Akt Regulates a Rab11-Effector Switch Required for Ciliogenesis. Developmental Cell *50*, 229-246.e7. https://doi.org/10.1016/j.devcel.2019.05.022.

106. Lai, S.-L., Yao, W.-L., Tsao, K.-C., Houben, A.J.S., Albers, H.M.H.G., Ovaa, H., Moolenaar, W.H., and Lee, S.-J. (2012). Autotaxin/Lpar3 signaling regulates Kupffer's vesicle formation and left-right asymmetry in zebrafish. Development *139*, 4439–4448. https://doi.org/10.1242/dev.081745.
107. Lin, Y.-N., Audira, G., Malhotra, N., Ngoc Anh, N.T., Siregar, P., Lu, J.-H., Lee, H., and Hsiao, C.-D. (2020). A Novel Function of the Lysophosphatidic Acid Receptor 3 (LPAR3) Gene in Zebrafish on Modulating Anxiety, Circadian Rhythm Locomotor Activity, and Short-Term Memory. IJMS *21*, 2837. https://doi.org/10.3390/ijms21082837.
108. Kusano, S., and Raab-Traub, N. (2002). I-mfa domain proteins interact with Axin and affect its regulation of the Wnt and c-Jun N-terminal kinase signaling pathways. Mol Cell Biol *22*, 6393–6405. https://doi.org/10.1128/MCB.22.18.6393-6405.2002.
109. Goto, T., Matsuzawa, J., Iemura, S.-I., Natsume, T., and Shibuya, H. (2016). WDR26 is a new partner of Axin1 in the canonical Wnt signaling pathway. FEBS Lett *590*, 1291–1303. https://doi.org/10.1002/1873-3468.12180.
110. Liu, W., Rui, H., Wang, J., Lin, S., He, Y., Chen, M., Li, Q., Ye, Z., Zhang, S., Chan, S.C., et al. (2006). Axin is a scaffold protein in TGF-beta signaling that promotes degradation of Smad7 by Arkadia. EMBO J *25*, 1646–1658. https://doi.org/10.1038/sj.emboj.7601057.
111. Zhang, K., Da Silva, F., Seidl, C., Wilsch-Bräuninger, M., Herbst, J., Huttner, W.B., and Niehrs, C. (2023). Primary cilia are WNT-transducing organelles whose biogenesis is controlled by a WNT-PP1 axis. Developmental Cell *58*, 139-154.e8. https://doi.org/10.1016/j.devcel.2022.12.006.
112. Stranneheim, H., Lagerstedt-Robinson, K., Magnusson, M., Kvarnung, M., Nilsson, D., Lesko, N., Engvall, M., Anderlid, B.-M., Arnell, H., Johansson, C.B., et al. (2021). Integration of whole genome sequencing into a healthcare setting: high diagnostic rates across multiple clinical entities in 3219 rare disease patients. Genome Med *13*, 40. https://doi.org/10.1186/s13073-021-00855-5.
113. Ek, M., Nilsson, D., Engvall, M., Malmgren, H., Thonberg, H., Pettersson, M., Anderlid, B.-M., Hammarsjö, A., Helgadottir, H.T., Arnardottir, S., et al. (2023). Genome sequencing with comprehensive variant calling identifies structural variants and repeat expansions in a large fraction of individuals with ataxia and/or neuromuscular disorders. Front. Neurol. *14*, 1170005. https://doi.org/10.3389/fneur.2023.1170005.
114. Wachten, D., and Mick, D.U. (2021). Signal transduction in primary cilia - analyzing and manipulating GPCR and second messenger signaling. Pharmacol. Ther. *224*, 107836. https://doi.org/10.1016/j.pharmthera.2021.107836.
115. Alvarez, L., Friedrich, B.M., Gompper, G., and Kaupp, U.B. (2014). The computational sperm cell. Trends in cell biology *24*, 198–207. https://doi.org/10.1016/j.tcb.2013.10.004.
116. Lázár, E., Mauron, R., Andrusivová, Ž., Foyer, J., He, M., Larsson, L., Shakari, N., Salas, S.M., Avenel, C., Sariyar, S., et al. (2024). Spatial Dynamics of the Developing Human Heart. Preprint, https://doi.org/10.1101/2024.03.12.584577 https://doi.org/10.1101/2024.03.12.584577.
117. Durinck, S., Spellman, P.T., Birney, E., and Huber, W. (2009). Mapping identifiers for the integration of genomic datasets with the R/Bioconductor package biomaRt. Nat Protoc *4*, 1184–1191. https://doi.org/10.1038/nprot.2009.97.
118. Nilsson, P., Paavilainen, L., Larsson, K., Ödling, J., Sundberg, M., Andersson, A.-C., Kampf, C., Persson, A., Szigyarto, C.A.-K., Ottosson, J., et al. (2005). Towards a human proteome atlas: High-throughput generation of mono-specific antibodies for tissue profiling. Proteomics *5*, 4327–4337. https://doi.org/10.1002/pmic.200500072.
119. Uhlen, M., Bandrowski, A., Carr, S., Edwards, A., Ellenberg, J., Lundberg, E., Rimm, D.L., Rodriguez, H., Hiltke, T., Snyder, M., et al. (2016). A proposal for validation of antibodies. Nat Methods *13*, 823–827. https://doi.org/10.1038/nmeth.3995.
120. Edfors, F., Hober, A., Linderbäck, K., Maddalo, G., Azimi, A., Sivertsson, Å., Tegel, H.,

Hober, S., Szigyarto, C.A.-K., Fagerberg, L., et al. (2018). Enhanced validation of antibodies for research applications. Nat Commun *9*, 4130. https://doi.org/10.1038/s41467-018-06642-y.
121. Virtanen, P., Gommers, R., Oliphant, T.E., Haberland, M., Reddy, T., Cournapeau, D., Burovski, E., Peterson, P., Weckesser, W., Bright, J., et al. (2020). SciPy 1.0: fundamental algorithms for scientific computing in Python. Nat Methods *17*, 261–272. https://doi.org/10.1038/s41592-019-0686-2.
122. Pedregosa, F., Varoquaux, G., Gramfort, A., Michel, V., Thirion, B., Grisel, O., Blondel, M., Prettenhofer, P., Weiss, R., Dubourg, V., et al. (2011). Scikit-learn: Machine Learning in Python. J. Mach. Learn. Res. *12*, 2825–2830.
123. Kolberg, L., Raudvere, U., Kuzmin, I., Adler, P., Vilo, J., and Peterson, H. (2023). g:Profiler—interoperable web service for functional enrichment analysis and gene identifier mapping (2023 update). Nucleic Acids Research *51*, W207–W212. https://doi.org/10.1093/nar/gkad347.
124. Wu, T., Hu, E., Xu, S., Chen, M., Guo, P., Dai, Z., Feng, T., Zhou, L., Tang, W., Zhan, L., et al. (2021). clusterProfiler 4.0: A universal enrichment tool for interpreting omics data. The Innovation *2*, 100141. https://doi.org/10.1016/j.xinn.2021.100141.
125. Gu, Z., and Hübschmann, D. (2023). *SimplifyEnrichment* : A Bioconductor Package for Clustering and Visualizing Functional Enrichment Results. Genomics, Proteomics & Bioinformatics *21*, 190–202. https://doi.org/10.1016/j.gpb.2022.04.008.
126. Danielsson, A., Pontén, F., Fagerberg, L., Hallström, B.M., Schwenk, J.M., Uhlén, M., Korsgren, O., and Lindskog, C. (2014). The Human Pancreas Proteome Defined by Transcriptomics and Antibody-Based Profiling. PLoS ONE *9*, e115421. https://doi.org/10.1371/journal.pone.0115421.
127. Uhlen, M., Oksvold, P., Fagerberg, L., Lundberg, E., Jonasson, K., Forsberg, M., Zwahlen, M., Kampf, C., Wester, K., Hober, S., et al. (2010). Towards a knowledge-based Human Protein Atlas. Nat Biotechnol *28*, 1248–1250. https://doi.org/10.1038/nbt1210-1248.
128. Kampf, C., Olsson, I., Ryberg, U., Sjöstedt, E., and Pontén, F. (2012). Production of Tissue Microarrays, Immunohistochemistry Staining and Digitalization Within the Human Protein Atlas. JoVE, 3620. https://doi.org/10.3791/3620.
129. Martinez Casals, A. (2023). Indirect immunofluorescence - tissue staining in TMA and whole tissue FFPE sections v1. Preprint, https://doi.org/10.17504/protocols.io.6qpvr4w6ogmk/v1.